THE ASTROPHYSICAL JOURNAL, 421:517–541, 1994 February 1

HST PHOTOMETRY OF THE TRAPEZIUM CLUSTER[1]

CHARLES F. PROSSER, JOHN R. STAUFFER, AND LEE HARTMANN
Smithsonian Astrophysical Observatory, 60 Garden Street, Cambridge, MA 02138
DAVID R. SODERBLOM
Space Telescope Science Institute, 3700 San Martin Drive, Baltimore, MD 21218
BURTON F. JONES
Lick Observatory, Board of Studies in Astronomy and Astrophysics, University of California, Santa Cruz, CA 95064
MICHAEL W. WERNER
Jet Propulsion Lab, M/S 169-327, 4800 Oak Drive, Pasadena, CA 91109
AND
MARK J. MCCAUGHREAN
Max-Planck-Institut für Astronomie, Königstuhl 17, W-6900 Heidelberg, Germany
Received 1993 May 25; accepted 1993 August 5

ABSTRACT

We have obtained images of 11 fields in the Trapezium cluster with the Planetary Camera (PC) of the *Hubble Space Telescope* in order to extend Herbig & Terndrup's (1986) study of this prototype, dense embedded cluster to fainter magnitudes than is possible from the ground. Using these images, we have identified 319 stars within an area of ~ 12 arcmin^2 corresponding roughly to a volume of ~ 0.065 pc^3 assuming the cluster is approximately spherically symmetric. Our completeness limits for star identification in V-band and I-band images are $V \simeq 20$ and $I_C \simeq 19$ respectively, corresponding to a mass limit of approximately 0.15 $M_\odot$ if the faintest stars have the same average A_V as that estimated for the brighter stars in the cluster. We have compared the V versus $V-I$ color-magnitude diagram derived from the *HST* photometry to new theoretical isochrones. Star formation in the Trapezium appears to be remarkably coeval, with $\geq 80\%$ of the stars having inferred ages less than 1 Myr. Over the somewhat limited mass range of the observations, there is no evidence for "bimodal" star formation—the high- and low-mass stars appear to have the same ages.

The sharp cores of the *HST* images and the small angular size of the PC pixels has allowed us to identify 35 new visual binaries in the cluster with separations from $\sim 0\farcs06$ (~ 26 AU) to $\sim 1\farcs0$ (~ 440 AU). For the range of binary separations that we are sensitive to, the observed binary frequency for the Trapezium is essentially identical to that estimated for field low-mass stars by Duquennoy & Mayor (1991). The most straightforward inference from this result is that binaries in this separation are unlikely to be formed by a tidal capture process.

We have also identified three stars which have associated compact nebulosity visible in the *HST* images. One of these star + nebulosity cases was previously identified by O'Dell, Wen, & Hu (1993)—these objects appear to form a class of objects whose circumstellar matter is being "lit up," most likely by θ^1 Ori C, enabling the gas to be observable at both optical and radio wavelengths (Felli et al. 1993a, b). We provide a brief summary of the optical properties of the other radio sources which appear in our PC images.

Subject headings: binaries: visual — ISM: individual (Orion Nebula) — open clusters and associations: individual (Trapezium) — stars: pre–main-squence

1. INTRODUCTION

The Trapezium cluster is one of the densest known star-forming regions in the Galaxy. Despite that distinction and the large number of astronomical observations in the Orion Nebula region to date, the cluster itself has not been extensively studied primarily because of the bright nebular background emission from the H II region that is excited by θ^1 Ori. The existence of a cluster of fainter stars surrounding θ^1 Ori was first demonstrated by Trümpler (1931), who obtained a red sensitive photograph of the region with the Crossley 36 inch reflector. Baade & Minkowsi (1937) obtained similar photographic evidence for the existence of a dense cluster around θ^1 Ori. A chronicle of the visual and photographic studies of the Trapezium cluster region is provided in Herbig (1982). Currently, the most complete proper motion study in the central Trapezium region is that of Jones & Walker (1988).

Herbig & Terndrup (1986, hereafter HT) provided the first quantitative study of the stellar content of the Trapezium cluster. They obtained narrow-band V and I CCD images of the cluster within an approximately 10 arcmin^2 region around θ^1 Ori, identified ~ 140 stars down to $I_C \sim 16$ mag, and estimated a density of ~ 2200 stars pc^{-3} for the cluster. Two other conclusions reached by HT were that: (1) with only a few exceptions, all of the Trapezium cluster stars have ages estimated at 10^6 yr or younger when compared to theoretical isochrones, and (2) despite this young age, only one of 10 stars observed spectroscopically appears to be a classical T Tauri star. HT speculated that the extremely high stellar density

[1] Based on observations with the NASA/ESA *Hubble Space Telescope*, obtained at the Space Telescope Science Institute, which is operated by the Association of Universities for Research in Astronomy, Inc., under NASA contract NAS5-26555.

might affect the properties of the stars via star-star or star-disk gravitational interactions.

Near-IR photometry of the Trapezium cluster region (McCaughrean et al. 1994) identified ~ 500 possible members within a 25 arcmin^2 region. A summary of their conclusions is provided in Zinnecker, McCaughrean, & Wilking (1992). A number of other near-IR imaging surveys have identified several other embedded, very dense clusters similar to but not as extreme as the Trapezium cluster. At least in L1630, Lada et al. (1991) believe that most stars may be formed in such dense clusters, though it is also likely that most such clusters become unbound prior to their becoming visible.

Larson (1990) and Clarke & Pringle (1991a, b) considered whether binary formation via star-disk collisions might be enhanced in a high-density region like the Trapezium. Their work also served to highlight the idea that disks might be truncated or removed in such an environment—and if disks are required to create the emission line spectra seen in classical T Tauri stars, then a deficiency of such disks might explain the deficiency of classical T Tauri stars seen by HT in the Trapezium cluster. Even if they do not disrupt disks or create binaries, star-disk encounters can have other effects—such as producing tilts between the disk angular momentum vector and the angular momentum vector of the central star. Heller (1993) suggested that the observed 7° tilt between the solar angular momentum vector and the planetary system angular momentum vector might best be explained by star-disk encounters if the Sun had been born in a dense cluster like the Trapezium.

The region near θ^1 Ori has also been studied for a variety of other reasons, some of which may be at least indirectly related to the Trapezium cluster itself. The BN-KL complex (Rieke, Low, & Kleinmann 1973; Wynn-Williams & Becklin 1974; Werner et al. 1976) is located within the angular confines of the cluster, though it is presumably embedded within the molecular cloud behind θ^1 Ori and is generally assumed to be younger than the Trapezium cluster members. VLA maps of the Trapezium region (Felli et al. 1993a) have identified ~ 40 compact radio sources. Many of these are nonthermal in nature and coincide with optical stars, plausibly indicating that these objects are late-type, flaring pre–main-sequence stars similar to those found in the ρ Oph region (Montmerle et al. 1983; Leous et al. 1991). Some of the compact sources with thermal radio spectra are associated with sources identified as nebular in the optical (Laques & Vidal 1979). One explanation for such objects is that they are circumstellar disks of low-mass cluster members, currently being illuminated by UV irradiation from θ^1 Ori (Churchwell et al. 1987; Garay, Moran, & Reid 1987). Using narrow-band *HST* images, O'Dell, Wen, & Hu (1993) have recently discovered several instances of stars associated with compact, often asymmetric, circumstellar nebulosity. They have interpreted these circumstellar nebulae as protoplanetary disks externally photoionized by $\theta^1 C$ Ori or one of the other O stars in the immediate vicinity. Meaburn et al. (1993) present observations of high-velocity flow patterns in the Trapezium cluster region and discuss whether the observed collimated outflows are the results of "jets" from young stellar objects or of a high-speed wind from $\theta^1 C$. Additional studies of the Trapezium region in the infrared and X-ray regimes are in progress (McCaughrean et al. 1994; Gagné et al. 1993).

A deeper photometric survey of the Trapezium cluster is needed in order to help interpret a number of the observational results obtained during the past few years. The bright H II region which envelops the Trapezium cluster makes *HST* the telescope of choice for such a project. The nebular surface brightness measured by HT in the region of the Trapezium stars is typically $I_C \sim 16$ mag arcsec^{-2}, making accurate photometry difficult for ground-based telescopes whose seeing disks are typically of order 1 arcsec. With the *HST* Planetary Camera observations, $\sim 15\%$ of the light from a star falls within a 0.″1 core, which when combined with the 0.″04 pixel^{-1} scale gives *HST* a 3–4 magnitude advantage for detecting stars relative to a typical ground-based image. Despite the difficulty imposed by the H II region, the Trapezium cluster is an exciting target to study for the reasons cited above and for one other reason. Previous detailed studies of stars forming regions have generally concentrated on associations—Taurus-Auriga, Chameleon, Sco-Cen, the more extended Orion population; these regions are certainly not bound and thus will not exist as identifiable entities by the time their low-mass stars evolve to the main sequence. There have been no detailed studies of $\sim 10^6$ year old populations that are dense enough to remain bound after their placental gas is removed. The Trapezium cluster may be dense enough to survive that stage (cf. HT), and thus study of its stars may allow us to determine if stellar properties are a function of the large-scale environment from which stars form. If that is so, the Trapezium stars would be the more relevant progenitors, rather than stars in associations like Taurus-Auriga, for studies of the time evolution of stars in open clusters (e.g., Stauffer & Hartmann 1987; Soderblom et al. 1993).

The specific goals of our *HST* study are (1) to extend the census of cluster members several magnitudes fainter than HT's survey, (2) to use the deeper census of cluster members to attempt to place better constraints on the time spread of star formation, (3) to determine the apparent binary frequency in the cluster on scales of less than 1 arcsec, and (4) to determine the mass function of the Trapezium cluster to as faint a limit as possible. In this paper, we will primarily address the first three issues; most of the discussion of the cluster mass function will be deferred to a later paper.

2. OBSERVATIONS

During 1991 August and September, the *Hubble Space Telescope* observed 12 fields in the inner Trapezium cluster region, using the Planetary Camera (PC). The approximate locations and orientations of these 12 fields are illustrated in Figure 1 (Plate 4), which is based on finding chart no. 6 of Jones & Walker (1988). We note that the *HST* observations and the ground-based observations of Herbig & Terndrup (1986) cover similar-sized, but slightly different areas—although they contain many stars in common (see § 4.1). Neither the present survey nor that by Herbig & Terndrup covers the entire cluster area. The PC images were obtained with the uncorrected optical system, and therefore suffered from the well-known spherical aberration in the point spread function (PSF). Table 1 lists the positions and dates of observation of the 12 fields. One field ("A") was a 1 s F547M ("V") exposure at the center of the Trapezium—the four bright stars constituting the Trapezium are themselves saturated in this exposure. The remaining 11 fields comprise the main results of our *HST* PC survey. For these 11 fields, each field has two 400 s and one 60 s exposure with the F547M ("*V*") filter, and one 500 s and one 23 s exposure with the F875M ("*I*") filter. Each field therefore has five different exposures, with the exception of fields "B" and "C" which have three additional exposures each (two 700 s

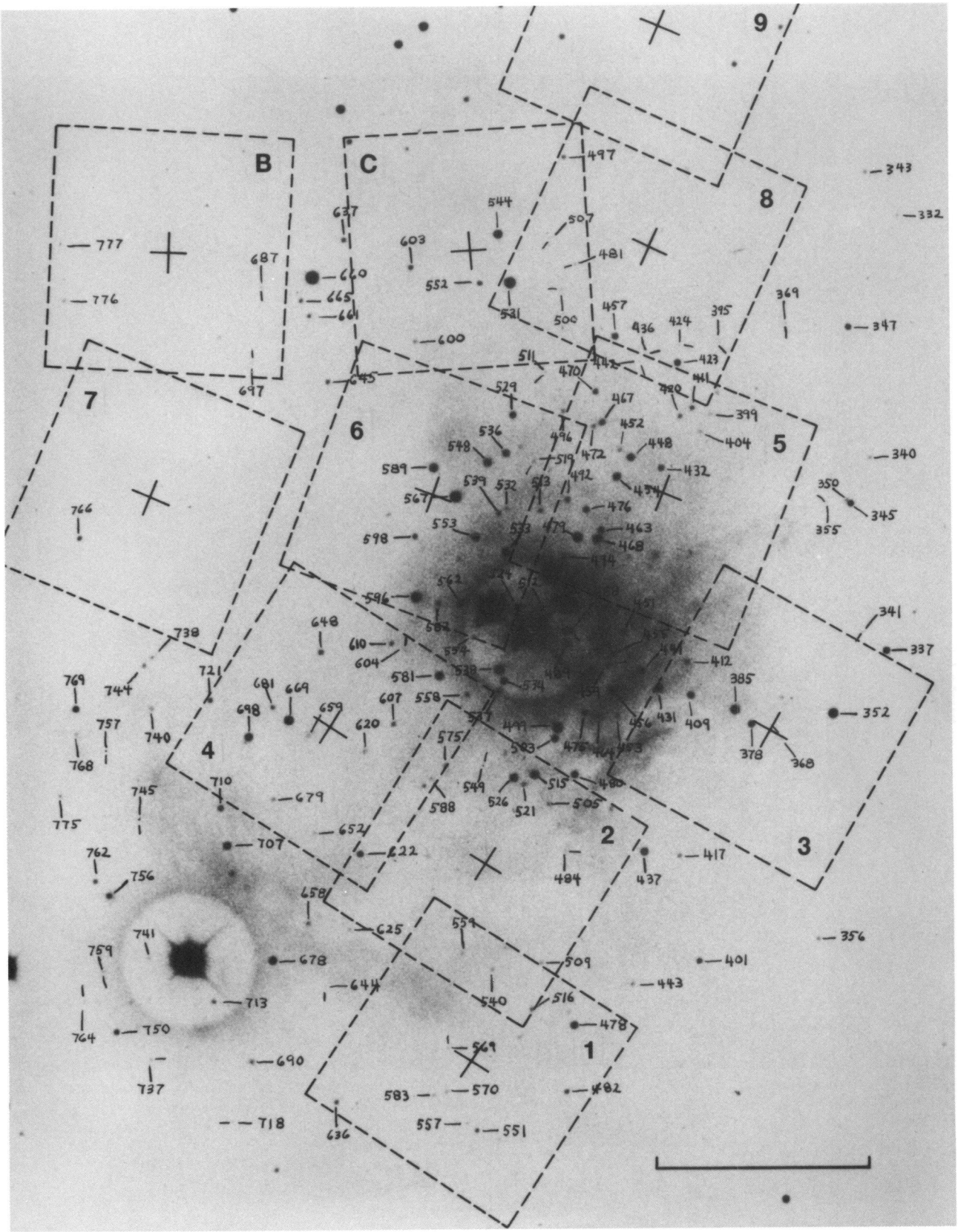

FIG. 1.—Approximate locations and orientations of the *HST* Planetary Camera Observations in the Trapezium cluster region (original chart is shown in Fig. 3*f* of Jones & Walker 1988). North is at top, east is to the left and the scale bar has length 1′. Each PC field has approximate dimensions 1′ × 1′. Numbers given for individual stars are their JW number identifications. This plate may be compared to Figure 6 in which the individual PC and JW star positions are plotted.

PROSSER et al. (see 421, 518)

TABLE 1

PLANETARY CAMERA FIELD POSITIONS

Field	R.A. (2000)	Decl.	UT Date
1 ...	$5^h35^m17^s.8$	$-5°25'12''$	1991 Aug 02
2 ...	5 35 17.4	−5 24 15	1991 Aug 02
3 ...	5 35 12.1	−5 23 36	1991 Aug 03
4 ...	5 35 20.4	−5 23 38	1991 Aug 03
5 ...	5 35 14.3	−5 22 31	1991 Aug 16
6 ...	5 35 18.7	−5 22 30	1991 Aug 11
7 ...	5 35 23.1	−5 22 32	1991 Aug 16
8 ...	5 35 14.4	−5 21 27	1991 Aug 04
9 ...	5 35 14.4	−5 20 22	1991 Aug 04
B ...	5 35 23.8	−5 21 28	1991 Sep 15
C ...	5 35 18.1	−5 21 26	1991 Sep 14
A ...	5 35 16.5	−5 23 23	1991 Jul 29

and one 140 s) with the F413M ("*B*") filter. The PC images are not normally oriented precisely along the α and δ axes on the sky, but are rotated slightly at an angle to these axes, depending on the telescope's roll angle at the time of observation. In a few cases, these exposure times were cut short due to loss of lock on the guide star, but the lost exposure time did not significantly affect the final results obtained.

The number of exposures and length of exposure time per field were constrained by the total amount of telescope time allocated for this program. This is the reason why only two fields were observed in B, for the existence of the extra 1 s *V* exposure of the central Trapezium "A" field, and for the relative number of long and short *V* and *I* exposures in each field. As the high cosmic-ray contamination makes distinctions between faint stars and cosmic rays difficult, it would have been preferable to take two 250 s *I* exposures per field instead of a single 500 s exposure, however time constraints prevented the use of this option.

3. DATA REDUCTION

All raw images were reduced using the standard STSDAS pipeline reduction program "calwfp" in the wfpc package of STSDAS. Table 2 lists the reference files used in the reduction of the Tapezium PC frames. Filenames for the Trapezium data are of the form "w0o70f0xt," where the field designation, "f," takes the value 1–9 and a–c, and the specific exposure designation, "x," has the values 1–5 for those fields with only *V* and *I* observations and the values 1–8 for those fields with additional exposures with the B filter. At the time of this analysis, on-orbit flat-field reference files did not exist for the filters used in this program. F547M has ground-based flat-field data, however F875M and F413M do not. After comparison of the results of different reductions in the three filters, including the use of on-orbit flat fields for other filters with passbands similar to our filters, we chose to employ the ground-based (or "prelaunch") F547M flat for the F547M images, the F814W (prelaunch) flat for the F875M images, and the F439W (preliminary on-orbit) flat for the F413M images. Among the main considerations in the decision of how to flat-field the data was the preference to remain with the exact same filter as the observations and the desire to not introduce new features into the image by application of the flat field. Some narrow-band on-orbit flat-fields of other filters tested in the reductions of our image in some cases did appear to introduce unwanted patterns or structure not seen when using the ground-based flat field of the same filter. Compared to ground-based flats with the same filter, the on-orbit flats will produce better representations of the actual CCD illumination—particularly near the edge of CCDs. The resulting photometric accuracy for such "edge" stars will likely be slightly worse than for stars near the center of the CCDs. Use of an on-orbit flat in the reductions would yield some slight improvement; however, we believe that the dominant sources of error in our photometry are the peculiar *HST* PSF and the variable background caused by the Trapezium H II region.

TABLE 2

PLANETARY CAMERA REFERENCE FILES

File Description	Name
Static mask	a4512124w
Analog to digital	a8h1350qw
Bias	b3s1244jw
Preflash	a8h15375w, a8h1537fw
Dark	a820853sw
F547M flat	a2q1021tw (F547M prelaunch)
F875M flat	a2q10528 (F814W prelaunch)
F413M flat	b3s1244mw (F439W preliminary on-orbit)

As has been noted previously (Holtzmann et al. 1991), charged particle detections or "cosmic-ray events" are a prominent feature of WFPC images—particularly for long exposures. Their removal from the image is complicated by the fact that one has to be careful not to also remove the central spike in the stellar PSFs. For the Trapezium data, a 2 × 6 pixel box was passed over each image, clipping those pixels within the box which were more than 5 σ above the box mean. A rectangular box was chosen in order to facilitate removal of streaks where several contiguous pixels may be bad. This "zapping" for cosmic-ray removal was run twice on each image and this successfully removed most of the bad pixels. After zapping, the stellar locations in each image were examined to be sure that no pixels in the central PSF profile were clipped. If any such pixels were clipped, the values were reset to the original values from the pre-zapped image. Any remaining bad pixels which may affect the background determinations for a star were removed interactively.

3.1. *Reduction Techniques*

Aperture photometry was performed using the DAOPHOT routines (Stetson 1987) incorporated into the current version of VISTA (Holtzmann et al. 1994). After some trial reductions, a small aperture radius of three pixels, with a background annulus region with radii from eight to 12 pixels, was chosen. At $\sim 0''.04$ pixel^{-1}, this corresponds to a $\sim 0''.12$ aperture radius and a background annulus of $0''.15$ width and inner radius $0''.32$. The benefits of applying such small aperture and use of background annuli which actually fall within the stellar PSF are discussed in Gilmozzi (1990). Some of the trial reductions involved use of a larger sky annulus (r = 60–70 pixels) to avoid most of the stellar PSF. For brighter stars with enough counts, there was essentially no difference between the small sky annulus (r = 8–12) and large sky annulus (r = 60–70) magnitudes, other than an offset. For fainter stars however, errors in the large sky annulus magnitudes increased—likely due to the presence of a variable background due to the nebu-

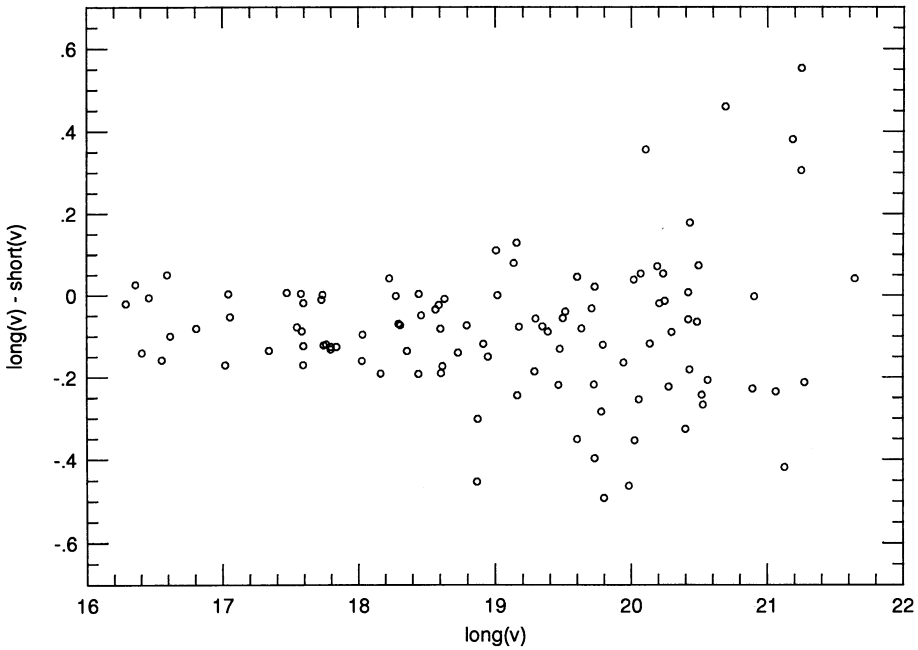

FIG. 2.—Instrumental magnitude differences between long and short exposures for 107 stars observed with the F547M filter, plotted vs. the instrumental "v" long exposure magnitude normalized to an exposure time of 60 s. A mean offset of −0.08 mag is found.

losity that exists on scale sizes similar to the large sky annulus. The spatially variable nebulosity encountered on the Trapezium images make the choice of a background annulus close to the core region where most counts are (rather than on the edge of the PSF) additionally appealing.

A set of "long" and "short" exposure aperture photometry magnitudes were created from the long and short exposures taken for each field. The "long V" magnitude was measured from the addition of the two ~400 s exposures for a field. The long and short instrumental magnitude systems were referenced to a 60 s exposure time. For each star, the long exposure magnitude was used, unless the star was saturated on the long exposure, in which case its magnitude from the short exposure was substituted. Figures 2 and 3 shows the comparison of the instrumental magnitudes for stars with measures from both long and short exposures, after removal of double stars and stars near the edge of the CCDs. The apparent systematic offset between the long- and short-magnitude systems in both V and I are clearly noticeable. The reason for this difference remains unclear; for the present we have applied a constant correction

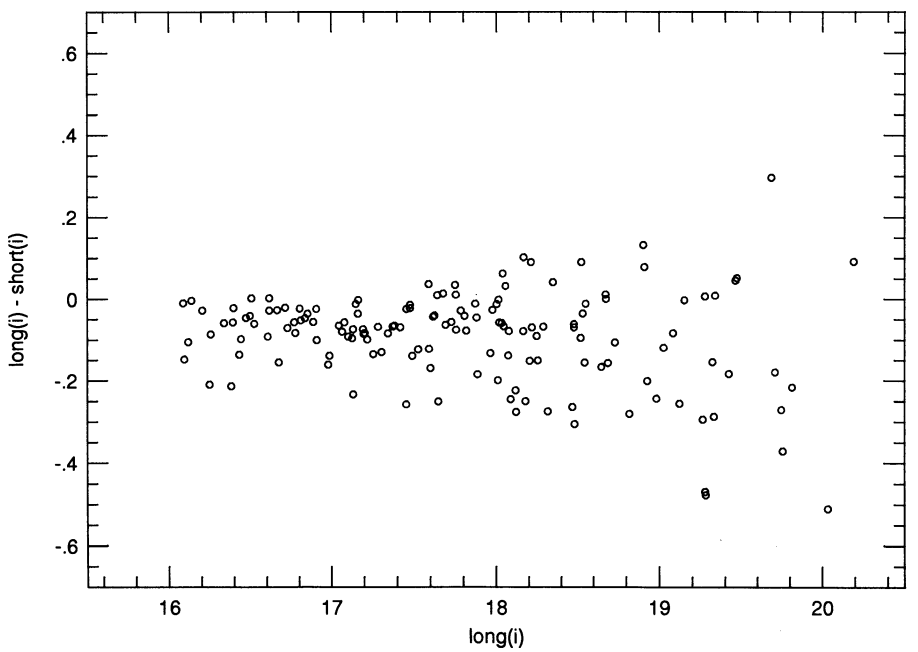

FIG. 3.—Same as Fig. 2, though for 147 stars observed with the F875M ("i") filter. A relative offset of −0.09 mag is found, similar to Fig. 2

to the short exposure magnitudes to bring all magnitudes into one system. Mean offsets of $\langle \Delta v \rangle_{l-s} = -0^m.08$ and $\langle \Delta i \rangle_{l-s} = -0^m.09$ were found from Figures 2 and 3.

The instrumental magnitudes were transformed onto a standard V, I_C system by use of 61 stars in common with the (V, I_C) CCD photometry of HT. Of the stars in common, 20 stars from HT have I_C magnitudes only, while 41 stars have (V, I_C) photometry. Dropping poorly fit stars, the linear transformations between instrumental (v, i) and standard (V, I_C) are

$$V = 1.035v - 1.354 \quad (30 \text{ stars}) \tag{1}$$

$$I_C = 1.055i - 3.116 \quad (49 \text{ stars}) . \tag{2}$$

While the transformation in V appeared sufficiently linear, there is the suggestion for I of an additional slight $V-I$ color term. Its affect is fairly small however, giving for an extreme case. $(v, i) = (22.5, 18.5)$, a $\Delta I = 0^m.27$ between linear and nonlinear transformations. As this difference is probably only slightly larger than the 1 σ error for this magnitude (see discussion below) we adopted the above linear transformations for this paper.

The standard deviation of the difference between our magnitudes and HTs for stars in common is $\sigma_v = 0^m.12$ (30 stars) and $\sigma_i = 0^m.14$ (49 stars). This external estimate of the accuracy of the *HST* photometry can be considered as an upper limit measure of the *HST* photometry accuracy, since there are additional contributing sources of error in the comparison between *HST* and HT (i.e., photometric errors in HT, intrinsic variability of these stars). Another measure of the accuracy can be obtained through internal comparisons. Using the stars shown in Figures 2 and 3, we can derive the uncertainties from comparison between the long- and short-exposure magnitudes. The long and short exposures for each field were taken contiguously and brightness variability influences were reduced. In Table 3 we show the 1 σ differences for the whole sample and for individual groups of bright and faint stars. In the brighter magnitude range we find typical 1 σ differences of $\sim 0^m.07$, while for lower S/N levels the accuracy degrades to $\sigma \sim 0^m.2$. The faintest stars ($V \geq 20.4$, $I \geq 18$) are likely to have uncertainties $\sigma \geq 0^m.2$ in V and I. If the long and short photometry is assumed to have equal measurement errors, then the 1 σ values in Table 3 would be multiplied by an additional factor of $1/2^{1/2}$ to derive the individual measurement error of one observation.

Duplicate observations of the same star provide another means to assess accuracy. Comparison of those stars observed in more than one field by *HST* (discussed below) yield $\sigma_{\Delta v} \simeq 0^m.19/2^{1/2} = 0^m.13$ (23 stars) and $\sigma_{\Delta i} = 0^m.17/2^{1/2} = 0^m.12$ (29 stars). The accuracies found are slightly worse than those from the long/short-exposure magnitude comparison likely due to the fewer numbers of stars and the fact that some doubles and near edge stars were included.

TABLE 3

ROOT MEAN SQUARE DIFFERENCES BETWEEN SHORT- AND LONG-EXPOSURE MAGNITUDES

Magnitude Range	Number of Stars	$< \Delta mag >$	$\sigma_{\Delta mag}$
V:			
All stars	107	−0.083	0.170
v < 18.7 (V<18)	43	−0.077	0.071
v ≥ 18.7 (V≥18)	64	−0.087	0.213
I:			
All stars	147	−0.091	0.115
i < 18.1 (I<16)	94	−0.072	0.066
i ≥ 18.1 (I≥16)	53	−0.124	0.165

3.2. *Photometric Data*

In Table 4 we present the main results of the *HST* observations—the V, I photometry for the 11 Trapezium fields. The columns in Table 4 give a running PC id number, a cross-reference JW id and proper motion membership probability (Jones & Walker 1988), the corresponding Parenago (1954) identification, and the V, I_C, and $V-I_C$ *HST* photometry. 2000 coordinates are given both in the conventional manner and in decimal degrees for use with Figures 6, 16, and 17. Also in Table 4 we have flagged those stars which lie near (within ~50 pixels) the edges or corners of the CCDs (= "*E*" flag), as their photometry may have slightly higher inaccuracies than stars near the center of the CCD. The flag "G" denotes objects which appear in the PC images, but which we believe are in fact "ghosts" or reflections arising in the PC (Burrows 1992). Objects were flagged as ghosts in cases where the image profile was noticeably different in appearance (unusually elongated for example) than for other stars observed near the same position, and where there were two or more such objects showing unusual PSFs and approximately aligned with a bright (saturated) star on the same CCD. The "V" flag denotes stars for which only upper limits in their V magnitudes could be obtained (i.e., the star has a V mag fainter than the value listed). Three nonstellar objects are flagged with "N." The "vi" column denotes from what exposure system (short = s, long = l) the V, I magnitudes for the object were taken; short exposure magnitudes were employed when saturation or other problems occurred for long exposures. Finally, the last column provides additional notes. Of the 326 stars/objects listed in Table 4, seven of these are considered as "ghosts," leaving a total of 319 stars having been detected.

The coordinates were determined using the xy2rd STSDAS program using input (x, y) coordinate positions together with the pointing information contained in the image headers. We can examine the accuracy of the positions computed from xy2rd in two ways: (1) comparison of coordinates for stars observed on more than one frame, and (2) comparison of these PC coordinates to the coordinates given in Jones & Walker (1988) for stars in common.

Comparison of the coordinates for multiple observations of the same star (discussed below) yield mean differences in α and δ of 0.35 and 0.63 arcsec, respectively. The comparison between the PC coordinates and those of JW are shown in Figures 4 and 5, where the relative differences in α and δ are illustrated for each of the four Planetary Camera CCDs. The mean offset between the JW and PC coordinates in α corresponds to the same sort of offset seen by HT. Such an offset is also seen when comparing the JW coordinates to VLA coordinates (Felli et al. 1993a) for nonthermal (stellar) sources in the Trapezium. It likely reflects a small zero-point error in the JW coordinates system. Figures 4 and 5 reveal that there is a significant spread, when compared to 1 PC pixel (~0.04 arcsec), in the coordinate difference both within a given CCD frame and between frames. Therefore, since we can measure the position of the stellar PSF core to an accuracy generally better than 1 pixel in each axis, the primary sources of positional error seen must be external to our own data analysis. These sources likely include errors in the boresight position of the PC camera as tabulated in the

TABLE 4

HST TRAPEZIUM PHOTOMETRY

PC	JW	Prob.	Par	V	I_C	V−I_C	RA (2000)	DEC	RA	DEC	Flag	Exp. vi	Notes
1	...	...	...	24.5	19.01	5.5	5 35 09.58	−5 23 55.9	83.7899	−5.3989	EV	ll	
2	...	...	...	20.27	16.05	4.22	5 35 09.82	−5 23 38.5	83.7909	−5.3940	...	ll	
3	...	...	...	22.0	19.82	2.2	5 35 09.84	−5 23 59.0	83.7910	−5.3997	V	ll	
4	349	0	...	18.45	16.53	1.92	5 35 10.44	−5 24 16.2	83.7935	−5.4045	...	ll	
5	352	99	1784	12.46	10.36	2.09	5 35 10.65	−5 23 44.8	83.7944	−5.3958	...	ss	
6	366	98	...	18.97	14.99	3.98	5 35 11.55	−5 24 21.0	83.7981	−5.4058	...	ll	
7	368	99	...	...	15.29	...	5 35 11.63	−5 23 51.2	83.7984	−5.3976	E	l	badpix for V
8	...	...	...	17.87	14.18	3.69	5 35 11.63	−5 23 40.8	83.7985	−5.3947	E	ll	
9	...	...	...	21.38	16.41	4.97	5 35 11.91	−5 22 53.9	83.7996	−5.3816	E	ll	in corner
10	373	99	...	16.85	13.48	3.37	5 35 11.91	−5 20 33.5	83.7996	−5.3426	...	ls	
11	378a	99	1808	15.00	12.89	2.11	5 35 12.17	−5 23 48.2	83.8007	−5.3967	E	ss	
12	378b	99	1808	15.81	13.49	2.32	5 35 12.17	−5 23 48.2	83.8007	−5.3967	E	ss	
13	377a	83	...	19.57	15.30	4.27	5 35 12.19	−5 20 45.7	83.8008	−5.3460	E	ll	
14	377b	83	...	20.96	16.31	4.65	5 35 12.20	−5 20 45.7	83.8008	−5.3460	E	ll	
15	...	...	...	...	18.11	...	5 35 12.31	−5 20 47.8	83.8013	−5.3466	E	l	
16	...	...	...	22.2	19.05	3.2	5 35 12.33	−5 21 32.2	83.8014	−5.3589	V	ll	
17	...	...	...	22.0	19.63	2.4	5 35 12.33	−5 21 32.0	83.8014	−5.3589	V	ll	
18	...	...	...	22.73	17.76	4.97	5 35 12.52	−5 23 01.8	83.8021	−5.3838	...	ll	
19	385	99	1807	12.64	11.02	1.62	5 35 12.52	−5 23 44.7	83.8021	−5.3957	E	ss	
20	382	99	...	18.12	15.24	2.88	5 35 12.53	−5 20 43.5	83.8022	−5.3454	E	ll	near poor column
21	389	52	...	19.49	15.85	3.64	5 35 12.71	−5 20 35.4	83.8029	−5.3432	...	ll	
22	390	99	...	17.60	15.05	2.55	5 35 12.72	−5 20 39.6	83.8030	−5.3443	...	ll	
23	391	99	1806	...	12.49	...	5 35 12.74	−5 20 44.2	83.8031	−5.3456	E	s	
24	...	...	...	23.4	19.14	4.2	5 35 12.78	−5 21 04.9	83.8032	−5.3514	V	ll	
25	...	...	...	...	19.33	...	5 35 12.93	−5 20 52.8	83.8039	−5.3480	...	l	
26	395	99	...	19.37	15.32	4.05	5 35 12.96	−5 22 00.9	83.8040	−5.3669	...	ll	
27	394	99	...	18.82	14.98	3.85	5 35 12.98	−5 20 30.9	83.8041	−5.3419	...	ll	
28	...	...	...	21.12	17.20	3.91	5 35 12.99	−5 21 53.2	83.8041	−5.3648	...	ll	
29	...	...	...	17.49	14.21	3.28	5 35 13.02	−5 22 15.7	83.8042	−5.3710	...	ll	
30	...	...	...	20.45	16.46	3.99	5 35 13.03	−5 22 53.1	83.8043	−5.3814	...	ll	
31	...	...	...	...	15.65	...	5 35 13.05	−5 22 47.0	83.8044	−5.3797	E	l	
32	...	...	...	19.46	15.64	3.82	5 35 13.07	−5 21 14.0	83.8045	−5.3539	E	ll	
33	399b	99	...	20.65	16.77	3.88	5 35 13.14	−5 22 21.6	83.8047	−5.3727	...	ll	
34	399a	99	...	18.48	15.29	3.19	5 35 13.14	−5 22 21.9	83.8047	−5.3727	...	ll	
35	400	99	...	17.74	14.58	3.16	5 35 13.14	−5 20 52.7	83.8048	−5.3480	...	ll	
36	...	...	...	21.2	18.95	2.3	5 35 13.18	−5 20 41.9	83.8049	−5.3450	EV	ll	
37	...	...	...	21.0	17.26	3.7	5 35 13.21	−5 23 53.2	83.8051	−5.3981	V?	ll	V uncertain
38	...	...	...	20.64	15.89	4.75	5 35 13.23	−5 22 57.8	83.8051	−5.3827	...	ll	
39	403	...	...	21.02	16.13	4.89	5 35 13.25	−5 20 19.5	83.8052	−5.3388	...	ll	
40	...	...	...	22.4	17.68	4.7	5 35 13.27	−5 23 53.3	83.8053	−5.3981	V	ll	
41	404	99	...	18.03	14.65	3.39	5 35 13.32	−5 22 26.8	83.8055	−5.3741	...	ll	
42	409	98	1824	14.46	12.55	1.90	5 35 13.34	−5 23 40.3	83.8056	−5.3945	E	ss	
43	...	...	...	...	17.48	...	5 35 13.39	−5 21 08.0	83.8058	−5.3522	E	l	
44	412	99	...	16.81	13.98	2.83	5 35 13.46	−5 23 31.5	83.8061	−5.3921	...	ll	
45	...	...	...	20.08	15.91	4.17	5 35 13.46	−5 23 04.4	83.8061	−5.3846	...	ll	
46	411	99	1820	16.13	13.54	2.58	5 35 13.47	−5 22 20.2	83.8061	−5.3723	E	ls	
47	...	...	...	20.66	16.42	4.24	5 35 13.53	−5 20 32.1	83.8064	−5.3423	...	ll	
48	...	...	...	19.69	16.27	3.42	5 35 13.56	−5 21 21.9	83.8065	−5.3561	E	ll	
49	...	...	...	20.11	17.89	2.22	5 35 13.58	−5 21 21.7	83.8066	−5.3560	E	ll	
50	420	99	1821	16.86	13.60	3.25	5 35 13.70	−5 22 22.7	83.8071	−5.3730	...	ls	
51	423	99	1819	14.40	12.30	2.09	5 35 13.73	−5 22 07.1	83.8072	−5.3686	...	ss	
52	424	94	...	19.42	15.61	3.81	5 35 13.74	−5 22 02.9	83.8073	−5.3675	...	ll	
53	...	...	...	21.59	16.37	5.22	5 35 13.92	−5 21 24.1	83.8080	−5.3567	...	ll	
54	431	97	1823	15.28	12.51	2.77	5 35 13.95	−5 23 38.4	83.8081	−5.3940	E	ss	
55	432	99	1822	16.30	13.04	3.26	5 35 14.03	−5 22 37.3	83.8085	−5.3770	...	ls	
56	...	...	...	...	19.49	...	5 35 14.10	−5 20 24.3	83.8088	−5.3401	...	l	
57	435a	...	...	19.30	15.70	3.60	5 35 14.17	−5 20 05.1	83.8091	−5.3347	...	ll	
58	435b	...	...	...	19.20	...	5 35 14.22	−5 20 04.5	83.8092	−5.3346	...	l	
59	436a	...	...	20.93	16.97	3.96	5 35 14.23	−5 22 04.5	83.8093	−5.3679	...	ll	
60	436b	...	...	21.31	17.52	3.79	5 35 14.25	−5 22 04.4	83.8094	−5.3679	...	ll	
61	...	...	...	21.7	17.35	4.4	5 35 14.26	−5 23 08.2	83.8094	−5.3856	V	ll	
62	...	...	...	...	17.65	...	5 35 14.29	−5 22 54.6	83.8096	−5.3818	...	l	
63	...	...	...	23.3	18.38	4.9	5 35 14.32	−5 22 36.9	83.8096	−5.3769	V	ll	
64	...	...	...	...	18.05	...	5 35 14.32	−5 22 56.2	83.8097	−5.3823	...	l	
65	442	99	...	18.61	15.33	3.28	5 35 14.49	−5 22 07.4	83.8104	−5.3687	...	ll	
66	...	...	...	22.5	17.22	5.3	5 35 14.55	−5 22 01.0	83.8106	−5.3669	V	ll	
67	445b	26	...	21.68	16.03	5.65	5 35 14.57	−5 20 43.3	83.8107	−5.3454	...	ll	
68	445a	26	...	18.92	14.67	4.24	5 35 14.58	−5 20 42.9	83.8107	−5.3453	...	ll	
69	...	...	...	19.12	15.45	3.67	5 35 14.60	−5 23 02.4	83.8108	−5.3840	...	ll	
70	448	99	1839	14.58	12.10	2.49	5 35 14.61	−5 22 34.6	83.8109	−5.3763	...	ss	

TABLE 4—*Continued*

PC	JW	Prob.	Par	V	I_C	V−I_C	RA (2000)	DEC	RA	DEC	Flag	Exp. vi	Notes
71	...	...	...	22.81	17.75	5.06	5 35 14.68	−5 21 07.2	83.8111	−5.3520	...	ll	
72	450	...	...	20.64	16.24	4.40	5 35 14.69	−5 20 29.9	83.8112	−5.3416	E	ll	
73	...	...	...	20.14	17.83	2.31	5 35 14.74	−5 23 05.3	83.8114	−5.3848	...	ll	
74	...	...	...	22.1	18.21	3.9	5 35 14.77	−5 22 24.0	83.8116	−5.3733	V	ll	
75	...	...	...	21.20	16.38	4.82	5 35 14.81	−5 23 05.6	83.8117	−5.3849	...	ll	
76	452	99	...	17.57	14.61	2.95	5 35 14.82	−5 22 32.5	83.8117	−5.3757	...	ll	
77	...	...	...	18.18	14.40	3.78	5 35 14.82	−5 24 11.6	83.8118	−5.4032	...	ll	
78	454	99	1840	13.96	11.86	2.09	5 35 14.85	−5 22 39.6	83.8119	−5.3777	E	ss	
79	...	...	...	18.60	15.29	3.30	5 35 14.85	−5 24 12.7	83.8119	−5.4035	...	ll	
80	...	...	...	18.14	14.86	3.27	5 35 14.85	−5 24 12.8	83.8119	−5.4035	...	ll	
81	...	...	...	22.8	19.75	3.1	5 35 14.89	−5 22 21.9	83.8120	−5.3728	V	ll	
82	457	79	1837	14.49	12.53	1.96	5 35 14.92	−5 22 00.7	83.8122	−5.3669	E	ss	
83	...	...	...	23.1	18.15	5.0	5 35 14.94	−5 21 48.0	83.8122	−5.3633	V	ll	
84	...	...	...	22.5	18.70	3.8	5 35 14.94	−5 20 53.2	83.8122	−5.3481	V	ll	
85	. .	...	...	20.68	17.58	3.10	5 35 14.98	−5 23 01.5	83.8124	−5.3837	V?	ll	
86	...	...	...	19.78	15.62	4.16	5 35 14.98	−5 22 32.0	83.8124	−5.3755	...	ll	
87	...	...	...	...	18.90	...	5 35 15.09	−5 20 48.8	83.8129	−5.3469	...	l	
88	...	...	...	20.75	18.35	2.40	5 35 15.12	−5 20 52.0	83.8130	−5.3478	V?	ll	
89	463	99	1841	14.26	12.12	2.14	5 35 15.13	−5 22 54.8	83.8130	−5.3819	...	ss	
90	461	...	...	22.18	16.82	5.36	5 35 15.16	−5 20 15.9	83.8132	−5.3378	...	ll	
91	467	99	1838	15.21	13.06	2.15	5 35 15.16	−5 22 25.0	83.8132	−5.3736	...	ss	
92	...	...	...	19.85	16.00	3.85	5 35 15.19	−5 20 29.6	83.8133	−5.3415	...	ll	
93	...	...	...	23.6	18.05	5.5	5 35 15.19	−5 21 56.3	83.8133	−5.3656	V	ll	
94	468	99	1842	13.16	11.50	1.67	5 35 15.20	−5 22 57.3	83.8133	−5.3826	...	ss	
95	...	...	...	...	19.24	...	5 35 15.28	−5 25 13.1	83.8137	−5.4203	G	l	ghost
96	...	...	...	19.73	15.30	4.43	5 35 15.29	−5 22 25.9	83.8137	−5.3739	...	ll	
97	470	99	...	15.17	12.54	2.63	5 35 15.31	−5 22 16.5	83.8138	−5.3712	...	ss	
98	472b	99	...	18.44	15.08	3.36	5 35 15.33	−5 22 26.2	83.8139	−5.3740	...	ll	
99	472a	99	...	18.12	14.84	3.28	5 35 15.33	−5 22 26.3	83.8139	−5.3740	...	ll	
100	...	...	...	22.03	19.11	2.92	5 35 15.34	−5 25 13.4	83.8139	−5.4204	G	ll	ghost
101	473	98	...	18.63	14.77	3.86	5 35 15.36	−5 21 15.0	83.8140	−5.3542	...	ll	
102	476	99	1861	16.04	13.34	2.70	5 35 15.42	−5 22 49.0	83.8142	−5.3803	...	ls	
103	478	99	1872	13.83	11.55	2.27	5 35 15.50	−5 25 14.5	83.8146	−5.4207	...	ss	
104	...	...	...	20.15	15.97	4.18	5 35 15.53	−5 22 59.3	83.8147	−5.3831	...	ll	
105	480	99	1871	14.51	12.44	2.08	5 35 15.55	−5 24 03.0	83.8148	−5.4008	E	ss	
106	479	99	1862	12.77	10.97	1.80	5 35 15.57	−5 22 56.9	83.8149	−5.3825	...	ss	
107	482	99	...	15.64	13.26	2.38	5 35 15.60	−5 25 33.6	83.8150	−5.4260	...	ss	
108	...	...	...	17.74	14.58	3.15	5 35 15.61	−5 25 10.9	83.8151	−5.4197	...	ll	
109	481	99	...	17.68	14.69	3.00	5 35 15.68	−5 21 40.4	83.8153	−5.3612	...	ll	
110	...	...	...	21.14	16.45	4.69	5 35 15.69	−5 24 11.5	83.8154	−5.4032	...	ll	
111	484a	99	...	18.96	15.78	3.18	5 35 15.69	−5 24 24.7	83.8154	−5.4069	...	ll	
112	484b	99	...	22.79	16.88	5.92	5 35 15.72	−5 24 24.7	83.8155	−5.4068	...	ll	
113	492	99	1860	17.11	13.83	3.28	5 35 15.77	−5 22 46.3	83.8157	−5.3795	...	ls	
114	...	...	...	...	18.98	...	5 35 15.79	−5 21 22.3	83.8158	−5.3562	...	l	
115	490	99	...	19.13	15.03	4.10	5 35 15.80	−5 20 41.0	83.8158	−5.3447	...	ll	
116	...	...	...	22.7	18.88	3.8	5 35 15.81	−5 24 31.2	83.8159	−5.4087	V	ll	
117	494	0:	...	15.92	13.56	2.36	5 35 15.82	−5 23 02.4	83.8159	−5.3840	...	ls	
118	...	...	...	18.79	16.49	2.30	5 35 15.83	−5 24 17.9	83.8160	−5.4050	...	ll	
119	...	...	...	20.60	16.17	4.43	5 35 15.84	−5 22 34.3	83.8160	−5.3762	E	ll	
120	496	0:	...	17.01	14.24	2.77	5 35 15.91	−5 22 21.2	83.8163	−5.3726	E	ll	
121	500	99	...	18.52	14.81	3.71	5 35 15.93	−5 21 47.6	83.8164	−5.3632	...	ll	
122	...	...	...	21.14	16.25	4.89	5 35 15.93	−5 20 22.1	83.8164	−5.3395	E	ll	
123	497	99	...	17.07	13.63	3.44	5 35 15.95	−5 21 10.1	83.8164	−5.3528	...	ls	
124	...	...	...	19.55	15.48	4.07	5 35 15.96	−5 25 51.0	83.8165	−5.4308	E	ll	
125	504b	99	1859	15.98	13.57	2.41	5 35 15.99	−5 20 36.9	83.8166	−5.3436	...	ss	
126	504a	99	1859	15.83	13.64	2.19	5 35 15.99	−5 20 36.8	83.8166	−5.3436	...	ss	
127	505	93	...	18.22	14.53	3.69	5 35 16.02	−5 24 11.6	83.8168	−5.4032	...	ll	
128	...	...	...	21.9	17.43	4.5	5 35 16.08	−5 22 55.7	83.8170	−5.3821	V	ll	
129	509a	99	...	18.48	15.06	3.42	5 35 16.09	−5 24 55.9	83.8170	−5.4155	...	ll	
130	509b	...	...	19.31	15.67	3.64	5 35 16.12	−5 24 55.5	83.8172	−5.4154	...	ll	
131	507	95	...	18.08	14.89	3.19	5 35 16.12	−5 21 32.9	83.8172	−5.3591	...	ll	
132	...	...	...	18.99	14.83	4.16	5 35 16.13	−5 22 37.8	83.8172	−5.3772	E	ll	
133	506	...	...	20.51	15.88	4.63	5 35 16.13	−5 21 11.2	83.8172	−5.3531	...	ll	
134	511b	99	...	...	17.99	...	5 35 16.21	−5 22 10.3	83.8175	−5.3695	E	l	
135	...	...	...	19.65	15.02	4.63	5 35 16.22	−5 21 09.5	83.8176	−5.3526	...	ll	
136	511a	99	...	19.47	15.67	3.80	5 35 16.23	−5 22 10.0	83.8176	−5.3695	E	ll	
137	510	95	...	19.21	15.28	3.93	5 35 16.24	−5 20 25.6	83.8177	−5.3405	E	ll	on bad column
138	...	...	...	21.0	17.49	3.5	5 35 16.27	−5 22 24.2	83.8178	−5.3734	V	ll	
139	513	99	...	17.09	14.15	2.94	5 35 16.27	−5 22 49.5	83.8178	−5.3804	...	ll	
140	...	...	...	19.90	15.88	4.03	5 35 16.28	−5 22 21.8	83.8178	−5.3727	...	ll	
141	516	99	...	17.29	14.34	2.95	5 35 16.31	−5 25 10.2	83.8180	−5.4195	...	ll	
142	...	...	...	20.32	16.05	4.27	5 35 16.31	−5 21 51.2	83.8180	−5.3642	...	ll	

TABLE 4—*Continued*

PC	JW	Prob.	Par	V	I_C	$V-I_C$	RA (2000)	DEC	RA	DEC	Flag	Exp. vi	Notes
143	519b	...	...	19.87	17.51	2.36	5 35 16.44	−5 22 35.8	83.8185	−5.3766	...	ll	
144	519a	...	...	17.77	14.30	3.47	5 35 16.45	−5 22 35.5	83.8185	−5.3765	...	ll	
145	...	...	...	23.13	18.08	5.05	5 35 16.46	−5 20 40.9	83.8186	−5.3447	...	ll	
146	521	86	...	18.48	14.32	4.16	5 35 16.51	−5 24 06.3	83.8188	−5.4017	E	ll	
147	...	...	...	17.76	14.62	3.14	5 35 16.52	−5 25 18.3	83.8188	−5.4217	...	ll	
148	...	...	...	22.14	17.23	4.91	5 35 16.52	−5 21 15.9	83.8188	−5.3544	...	ll	
149	...	...	...	...	19.26	...	5 35 16.56	−5 21 31.3	83.8190	−5.3587	...	l	
150	526b	98	1896	15.58	13.40	2.18	5 35 16.69	−5 24 04.4	83.8196	−5.4012	...	ss	
151	...	...	...	18.10	15.03	3.07	5 35 16.69	−5 22 31.6	83.8196	−5.3755	...	ll	
152	526a	98	1896	13.77	11.87	1.90	5 35 16.70	−5 24 04.5	83.8196	−5.4013	...	ss	
153	...	...	...	20.63	16.42	4.21	5 35 16.81	−5 23 06.9	83.8200	−5.3852	...	ll	
154	529	99	1886	14.90	12.40	2.50	5 35 16.86	−5 22 22.8	83.8202	−5.3730	...	ss	
155	...	...	...	...	17.79	...	5 35 16.86	−5 22 09.6	83.8203	−5.3693	E	l	
156	535	99	...	17.52	14.47	3.05	5 35 16.87	−5 25 47.0	83.8203	−5.4297	...	ll	
157	...	...	...	...	18.32	...	5 35 16.90	−5 21 29.9	83.8204	−5.3583	G?	l	real?
158	...	...	...	20.87	16.44	4.43	5 35 16.91	−5 22 21.1	83.8204	−5.3725	...	ll	
159	531	99	1885	...	9.99	...	5 35 16.91	−5 21 45.1	83.8205	−5.3625	...	s	
160	532	0:	...	19.15	15.53	3.62	5 35 16.92	−5 22 49.0	83.8205	−5.3803	N	ll	nonstellar
161	533	99	1888	15.06	12.62	2.44	5 35 16.92	−5 23 00.8	83.8205	−5.3836	...	ss	
162	...	...	...	...	13.74	...	5 35 16.96	−5 23 20.6	83.8207	−5.3891	G	l	ghost
163	...	...	...	19.88	15.83	4.05	5 35 17.00	−5 21 24.2	83.8208	−5.3567	...	ll	
164	...	...	...	14.40	14.05	0.35	5 35 17.00	−5 23 20.9	83.8208	−5.3891	G	sl	ghost
165	...	...	...	...	15.71	...	5 35 17.04	−5 23 20.0	83.8210	−5.3889	G	l	ghost
166	539	99	...	...	13.06	...	5 35 17.06	−5 22 49.9	83.8211	−5.3805	E	s	
167	...	...	...	...	18.35	...	5 35 17.07	−5 21 42.4	83.8211	−5.3618	G	l	ghost
168	540	99	...	18.63	14.55	4.07	5 35 17.07	−5 24 59.3	83.8211	−5.4165	...	ll	
169	...	...	...	...	17.45	...	5 35 17.12	−5 21 41.2	83.8214	−5.3614	G	l	ghost
170	544	99	1884	13.04	10.82	2.22	5 35 17.15	−5 21 32.2	83.8214	−5.3590	...	ss	
171	...	...	...	18.26	15.09	3.17	5 35 17.18	−5 24 24.6	83.8216	−5.4068	E	ll	
172	551b	99	...	16.92	14.36	2.56	5 35 17.28	−5 25 44.7	83.8220	−5.4291	...	ss	
173	551a	99	...	16.60	13.87	2.73	5 35 17.29	−5 25 44.7	83.8221	−5.4291	...	ss	
174	548	99	1909	16.29	13.91	2.38	5 35 17.31	−5 22 36.2	83.8221	−5.3767	...	ll	
175	...	...	...	...	16.64	...	5 35 17.32	−5 23 04.7	83.8222	−5.3846	...	l	
176	...	...	...	19.89	15.68	4.21	5 35 17.32	−5 24 14.2	83.8222	−5.4039	...	ll	
177	549	48	...	18.79	15.22	3.57	5 35 17.32	−5 24 00.5	83.8222	−5.4001	...	ll	
178	...	...	...	...	17.76	...	5 35 17.33	−5 23 41.6	83.8222	−5.3949	E	l	
179	...	...	...	19.79	15.47	4.32	5 35 17.40	−5 24 17.7	83.8225	−5.4049	...	ll	
180	...	...	...	15.82	13.28	2.54	5 35 17.41	−5 23 21.0	83.8225	−5.3892	...	ls	
181	...	...	...	18.71	15.50	3.22	5 35 17.43	−5 22 51.2	83.8226	−5.3809	...	ll	
182	557	99	...	16.86	14.18	2.68	5 35 17.47	−5 25 42.7	83.8228	−5.4285	...	ll	
183	552a	99	1908	17.15	14.50	2.65	5 35 17.49	−5 21 45.3	83.8229	−5.3626	E	ll	
184	552b	99	1908	19.21	15.96	3.25	5 35 17.50	−5 21 45.7	83.8229	−5.3627	E	ll	
185	553a	99	1911	14.91	12.41	2.49	5 35 17.50	−5 22 56.7	83.8229	−5.3824	...	ss	
186	553b	99	1911	16.85	14.93	1.91	5 35 17.53	−5 22 56.8	83.8230	−5.3824	...	ss	
187	...	...	...	20.55	16.21	4.34	5 35 17.59	−5 22 07.7	83.8233	−5.3688	E	ll	
188	...	...	...	19.66	15.93	3.73	5 35 17.60	−5 22 51.5	83.8233	−5.3810	...	ll	
189	...	...	...	18.71	16.38	2.33	5 35 17.60	−5 25 11.4	83.8233	−5.4198	...	ll	
190	558	98	...	18.29	15.73	2.56	5 35 17.60	−5 23 40.8	83.8233	−5.3947	N	ll	nonstellar
191	...	...	...	...	19.13	...	5 35 17.63	−5 25 40.8	83.8235	−5.4280	...	l	
192	...	...	...	19.67	15.62	4.05	5 35 17.64	−5 24 43.2	83.8235	−5.4120	E	ll	
193	559	55	...	18.86	14.69	4.17	5 35 17.65	−5 24 54.8	83.8235	−5.4152	...	ll	
194	...	...	...	...	16.34	...	5 35 17.67	−5 23 14.7	83.8236	−5.3874	...	l	
195	...	...	...	...	17.43	...	5 35 17.69	−5 23 42.4	83.8237	−5.3951	...	l	
196	...	...	...	19.93	15.55	4.38	5 35 17.70	−5 23 44.1	83.8238	−5.3956	...	ll	
197	...	...	...	...	19.17	...	5 35 17.71	−5 22 31.5	83.8238	−5.3754	...	l	
198	...	...	...	21.65	16.74	4.91	5 35 17.72	−5 24 41.2	83.8238	−5.4114	E	ll	
199	...	...	...	20.06	15.37	4.69	5 35 17.72	−5 24 30.6	83.8238	−5.4085	...	ll	
200	562	17	1912	15.68	13.01	2.67	5 35 17.76	−5 23 15.5	83.8240	−5.3876	...	ls	
201	...	...	...	16.84	14.41	2.43	5 35 17.81	−5 23 03.0	83.8242	−5.3842	...	ll	
202	570a	99	...	17.85	14.73	3.12	5 35 17.87	−5 25 34.6	83.8244	−5.4263	E	ll	
203	570b	99	...	18.81	15.28	3.53	5 35 17.87	−5 25 34.4	83.8244	−5.4262	E	ll	
204	...	...	...	20.48	15.92	4.56	5 35 17.88	−5 25 07.2	83.8245	−5.4187	...	ll	
205	569	92	...	18.93	14.72	4.21	5 35 17.88	−5 25 22.1	83.8245	−5.4228	E	ll	
206	...	...	...	20.93	16.18	4.75	5 35 17.89	−5 23 35.4	83.8245	−5.3932	...	ll	
207	567	99	1910	11.39	9.66	1.72	5 35 17.89	−5 22 45.3	83.8246	−5.3792	E	ss	
208	...	...	...	20.12	15.93	4.20	5 35 17.89	−5 23 35.3	83.8246	−5.3931	...	ll	
209	...	...	...	19.06	15.30	3.76	5 35 17.94	−5 22 05.8	83.8248	−5.3683	...	ll	
210	...	...	...	21.18	15.65	5.54	5 35 17.97	−5 24 03.5	83.8249	−5.4010	...	ll	
211	...	...	...	19.4	16.91	2.5	5 35 17.97	−5 23 30.7	83.8249	−5.3919	NV	ll	nonstellar
212	575	94	...	17.90	14.30	3.60	5 35 18.00	−5 24 01.5	83.8250	−5.4004	...	ll	

TABLE 4—*Continued*

PC	JW	Prob.	Par	V	I_C	V−I_C	RA (2000)	DEC	RA	DEC	Flag	Exp. vi	Notes
213	...	...	...	19.64	15.44	4.20	5 35 18.11	−5 24 30.4	83.8255	−5.4084	...	ll	
214	...	...	...	...	17.37	...	5 35 18.12	−5 23 31.4	83.8255	−5.3921	...	l	
215	...	...	...	...	18.91	...	5 35 18.13	−5 23 46.2	83.8255	−5.3962	...	l	
216	581	99	1913	13.92	11.58	2.34	5 35 18.13	−5 23 35.8	83.8255	−5.3933	...	ss	
217	583	0	...	16.18	14.48	1.70	5 35 18.14	−5 25 35.6	83.8256	−5.4266	...	ll	
218	582	99	...	18.65	14.96	3.69	5 35 18.18	−5 23 15.5	83.8258	−5.3876	...	ll	
219	...	...	...	19.63	16.19	3.43	5 35 18.19	−5 24 38.9	83.8258	−5.4108	...	ll	
220	...	...	...	20.19	15.59	4.60	5 35 18.22	−5 23 07.3	83.8259	−5.3854	...	ll	
221	...	...	...	20.61	16.72	3.89	5 35 18.24	−5 24 39.0	83.8260	−5.4108	...	ll	
222	...	...	...	19.97	16.13	3.84	5 35 18.26	−5 24 26.9	83.8261	−5.4075	...	ll	
223	588	87	...	19.46	15.92	3.54	5 35 18.26	−5 24 05.3	83.8261	−5.4015	...	ll	
224	...	...	...	19.11	15.16	3.94	5 35 18.28	−5 24 26.8	83.8262	−5.4075	...	ll	
225	...	...	...	19.63	16.21	3.43	5 35 18.29	−5 21 44.4	83.8262	−5.3623	...	ll	
226	589	99	1925	13.42	11.30	2.12	5 35 18.32	−5 22 38.2	83.8263	−5.3773	E	ss	
227	...	...	...	20.16	16.00	4.16	5 35 18.37	−5 25 19.8	83.8265	−5.4222	E	ll	
228	...	...	...	17.05	13.91	3.14	5 35 18.40	−5 24 07.5	83.8267	−5.4021	...	ll	= A24
229	...	...	...	...	19.13	...	5 35 18.41	−5 23 57.7	83.8267	−5.3994	...	l	
230	...	...	...	21.05	15.95	5.09	5 35 18.43	−5 23 29.3	83.8268	−5.3915	...	ll	
231	...	...	...	23.8	17.87	5.9	5 35 18.54	−5 22 31.6	83.8272	−5.3755	V	ll	
232	...	...	...	19.07	15.53	3.53	5 35 18.59	−5 23 56.4	83.8274	−5.3990	...	ll	
233	596	99	1927	15.58	13.06	2.52	5 35 18.61	−5 23 13.9	83.8275	−5.3872	...	ls	
234	598b	...	1926	...	16.69	...	5 35 18.63	−5 22 55.9	83.8276	−5.3822	E	s	
235	598a	99	1926	15.75	13.05	2.71	5 35 18.65	−5 22 56.7	83.8277	−5.3824	E	ls	
236	600	99	...	17.45	14.22	3.23	5 35 18.68	−5 22 02.4	83.8278	−5.3673	...	ll	
237	603	99	1924	15.63	13.42	2.21	5 35 18.77	−5 21 41.5	83.8282	−5.3615	...	ls	
238	...	...	...	20.39	15.58	4.81	5 35 18.79	−5 24 17.4	83.8283	−5.4048	E	ll	
239	...	...	...	...	17.54	...	5 35 18.80	−5 22 23.6	83.8283	−5.3732	...	l	
240	604	...	...	18.84	15.30	3.54	5 35 18.81	−5 23 29.0	83.8284	−5.3914	...	ll	
241	...	...	...	20.31	16.77	3.54	5 35 18.81	−5 22 23.8	83.8284	−5.3733	...	ll	
242	606	99	...	17.01	13.68	3.33	5 35 18.90	−5 21 08.6	83.8288	−5.3524	...	ls	
243	...	...	...	18.62	14.99	3.62	5 35 18.92	−5 22 19.5	83.8288	−5.3721	...	ll	
244	607	99	...	15.50	13.64	1.86	5 35 18.98	−5 23 49.7	83.8291	−5.3971	...	ls	
245	...	...	...	19.33	15.61	3.72	5 35 18.99	−5 25 03.9	83.8291	−5.4177	...	ll	
246	...	...	...	...	18.15	...	5 35 19.05	−5 23 06.9	83.8294	−5.3852	E	l	
247	610	99	1928	16.59	13.89	2.71	5 35 19.06	−5 23 27.1	83.8294	−5.3909	...	ll	
248	...	...	...	...	18.30	...	5 35 19.07	−5 21 43.9	83.8295	−5.3622	...	l	
249	...	...	...	22.4	17.22	5.2	5 35 19.09	−5 22 35.4	83.8296	−5.3765	V	ll	
250	...	...	...	17.03	14.23	2.80	5 35 19.15	−5 22 51.1	83.8298	−5.3809	...	ll	
251	617	...	...	20.99	16.58	4.41	5 35 19.43	−5 22 22.5	83.8310	−5.3729	...	ll	
252	616	95	...	20.18	15.75	4.43	5 35 19.45	−5 21 05.4	83.8310	−5.3515	E	ll	
253	620	99	...	17.00	14.41	2.58	5 35 19.51	−5 23 56.7	83.8313	−5.3991	E	ll	
254	622	99	1940	15.35	12.89	2.46	5 35 19.57	−5 24 26.6	83.8315	−5.4074	E	ss	
255	624	98	...	18.32	15.44	2.88	5 35 19.79	−5 22 22.5	83.8324	−5.3729	...	ll	
256	...	...	...	19.60	15.34	4.27	5 35 19.83	−5 24 02.1	83.8326	−5.4006	...	ll	= A121
257	...	...	...	...	18.31	...	5 35 19.93	−5 22 33.7	83.8331	−5.3760	E	l	
258	636	99	...	15.86	13.40	2.46	5 35 19.97	−5 25 38.1	83.8332	−5.4272	...	ss	
259	630	...	...	20.69	16.38	4.31	5 35 19.99	−5 22 27.4	83.8333	−5.3743	...	ll	
260	...	...	...	18.67	16.91	1.76	5 35 20.08	−5 25 34.3	83.8337	−5.4262	...	ll	
261	...	...	...	21.81	16.85	4.95	5 35 20.12	−5 22 29.3	83.8338	−5.3748	...	ll	
262	648b	99	1960	19.09	14.62	4.47	5 35 20.35	−5 23 30.0	83.8348	−5.3917	...	ls	
263	648a	99	1960	15.73	13.15	2.58	5 35 20.39	−5 23 30.2	83.8350	−5.3917	...	ls	
264	...	...	...	22.35	16.92	5.42	5 35 20.43	−5 23 31.5	83.8351	−5.3921	...	ll	near JW648AB
265	652	99	...	18.49	15.12	3.37	5 35 20.44	−5 24 20.4	83.8352	−5.4057	...	ll	
266	...	...	...	...	17.65	...	5 35 20.44	−5 23 23.4	83.8352	−5.3898	...	l	
267	659	84	...	18.18	14.03	4.15	5 35 20.57	−5 23 53.3	83.8357	−5.3982	...	ll	
268	656	...	...	21.51	17.27	4.24	5 35 20.57	−5 22 56.0	83.8357	−5.3822	...	ll	
269	657	...	...	19.80	16.12	3.68	5 35 20.58	−5 22 45.9	83.8357	−5.3794	...	ll	
270	...	...	...	20.67	16.18	4.49	5 35 20.67	−5 22 32.4	83.8361	−5.3757	...	ll	
271	...	...	...	19.40	15.75	3.66	5 35 20.84	−5 23 22.2	83.8369	−5.3895	...	ll	
272	...	...	...	21.02	15.95	5.08	5 35 20.92	−5 23 55.8	83.8371	−5.3988	...	ll	
273	669	99	1961	12.43	10.76	1.68	5 35 20.94	−5 23 49.1	83.8373	−5.3970	...	ss	
274	...	...	...	22.01	17.02	4.99	5 35 20.98	−5 22 23.8	83.8374	−5.3733	...	ll	
275	...	...	...	21.59	17.22	4.37	5 35 21.00	−5 22 26.2	83.8375	−5.3740	...	ll	
276	...	...	...	20.82	16.59	4.23	5 35 21.10	−5 24 00.3	83.8379	−5.4001	...	ll	
277	...	...	...	20.57	16.09	4.48	5 35 21.10	−5 23 33.6	83.8379	−5.3927	...	ll	
278	...	...	...	19.59	15.89	3.70	5 35 21.16	−5 21 59.9	83.8382	−5.3666	...	ll	
279	...	...	...	20.38	16.39	3.99	5 35 21.20	−5 23 46.2	83.8383	−5.3962	...	ll	within PSF of PC282
280	...	...	...	19.04	15.32	3.72	5 35 21.20	−5 22 60.0	83.8383	−5.3833	E	ll	
281	679	99	1991	16.86	14.48	2.38	5 35 21.23	−5 24 11.6	83.8384	−5.4032	...	ll	
282	681	99	...	16.26	13.86	2.40	5 35 21.26	−5 23 45.5	83.8386	−5.3960	...	ll	

TABLE 4—*Continued*

PC	JW	Prob.	Par	V	I_C	V−I_C	RA (2000)	DEC	RA	DEC	Flag	Exp. vi	Notes
283	...	...	...	...	16.83	...	5 35 21.27	−5 22 16.6	83.8386	−5.3713	E	l	
284	685	99	...	19.78	15.22	4.56	5 35 21.44	−5 23 17.1	83.8393	−5.3881	E	ll	
285	...	...	...	22.17	16.96	5.22	5 35 21.56	−5 23 26.2	83.8398	−5.3906	...	ll	
286	687b	54	...	...	17.32	...	5 35 21.60	−5 21 47.0	83.8400	−5.3631	...	l	
287	...	...	...	22.30	17.06	5.25	5 35 21.62	−5 23 48.5	83.8401	−5.3968	...	ll	
288	687a	54	...	17.67	14.66	3.00	5 35 21.62	−5 21 46.7	83.8401	−5.3630	...	ll	
289	694	99	...	17.73	14.74	2.99	5 35 21.70	−5 23 39.9	83.8404	−5.3944	E	ll	
290	698	99	1973	13.27	11.83	1.43	5 35 21.70	−5 23 54.0	83.8404	−5.3983	...	ss	
291	693	99	...	18.93	14.87	4.07	5 35 21.74	−5 23 11.1	83.8406	−5.3864	...	ll	
292	...	...	...	17.92	14.95	2.97	5 35 21.78	−5 23 55.6	83.8408	−5.3988	...	ll	
293	...	...	...	22.05	16.56	5.49	5 35 21.78	−5 22 41.4	83.8408	−5.3782	...	ll	
294	...	...	...	21.54	17.09	4.45	5 35 21.79	−5 23 06.9	83.8408	−5.3853	...	ll	
295	697	99	...	17.93	14.90	3.03	5 35 21.79	−5 22 08.0	83.8408	−5.3689	...	ll	
296	...	...	...	23.8	19.40	4.4	5 35 21.84	−5 23 07.8	83.8410	−5.3855	V	ll	
297	...	...	...	19.86	15.67	4.19	5 35 22.08	−5 22 35.3	83.8420	−5.3765	...	ll	
298	...	...	...	20.28	16.66	3.62	5 35 22.09	−5 22 13.2	83.8420	−5.3703	E	ll	
299	...	...	...	...	...	...	5 35 22.20	−5 22 18.6	83.8425	−5.3718	E	l	bad pixels
300	...	...	...	...	19.60	...	5 35 22.22	−5 21 42.2	83.8426	−5.3617	...	l	
301	712	99	...	16.73	14.12	2.61	5 35 22.39	−5 22 00.8	83.8433	−5.3669	...	ll	
302	...	...	...	...	19.32	...	5 35 22.43	−5 23 02.4	83.8435	−5.3840	...	l	
303	...	...	...	22.5	18.06	4.4	5 35 22.56	−5 21 37.8	83.8440	−5.3605	EV	ll	
304	...	...	...	...	18.02	...	5 35 22.65	−5 21 40.8	83.8444	−5.3613	...	l	
305	...	...	...	...	18.19	...	5 35 22.69	−5 21 57.4	83.8445	−5.3659	...	l	
306	723	99	...	17.89	14.72	3.17	5 35 22.75	−5 23 13.9	83.8448	−5.3872	...	ll	
307	...	...	...	22.03	17.28	4.76	5 35 22.80	−5 22 28.4	83.8450	−5.3745	...	ll	
308	726	99	...	19.24	15.35	3.89	5 35 22.92	−5 22 43.1	83.8455	−5.3786	E	ll	in corner
309	...	...	...	22.67	17.73	4.95	5 35 23.14	−5 22 29.7	83.8464	−5.3749	...	ll	
310	732	99	...	18.33	15.14	3.19	5 35 23.27	−5 21 25.9	83.8469	−5.3572	...	ll	
311	...	...	...	...	17.42	...	5 35 23.66	−5 22 14.2	83.8486	−5.3706	...	l	
312	...	...	...	...	17.81	...	5 35 23.83	−5 21 19.2	83.8493	−5.3553	...	l	
313	...	...	...	...	19.72	...	5 35 23.86	−5 23 01.5	83.8494	−5.3838	...	l	
314	748b	99	...	20.62	16.01	4.62	5 35 24.01	−5 21 33.3	83.8500	−5.3593	...	ll	
315	748a	99	...	17.91	14.77	3.14	5 35 24.03	−5 21 33.4	83.8501	−5.3593	...	ll	
316	...	...	...	20.73	16.10	4.63	5 35 24.05	−5 21 55.8	83.8502	−5.3655	...	ll	
317	...	...	...	22.5	18.22	4.2	5 35 24.30	−5 22 33.9	83.8513	−5.3761	V	ll	
318	761	98	...	22.33	16.60	5.74	5 35 24.60	−5 22 43.6	83.8525	−5.3788	...	ll	
319	...	...	...	...	18.63	...	5 35 24.66	−5 21 34.6	83.8528	−5.3596	...	l	
320	...	...	...	...	17.42	...	5 35 24.75	−5 21 57.9	83.8531	−5.3661	...	l	
321	766b	99	...	16.85	13.87	2.98	5 35 25.00	−5 22 59.6	83.8542	−5.3832	...	ls	
322	766a	99	...	16.37	13.64	2.73	5 35 25.01	−5 22 59.6	83.8542	−5.3832	...	ls	
323	776a	99	...	16.71	14.20	2.52	5 35 25.35	−5 21 51.7	83.8556	−5.3644	E	ls	
324	776b	99	...	19.77	15.85	3.92	5 35 25.39	−5 21 51.6	83.8558	−5.3643	E	ls	
325	777b	80	...	18.46	15.15	3.31	5 35 25.41	−5 21 35.3	83.8559	−5.3598	E	ll	
326	...	...	...	...	20.08	...	5 35 25.42	−5 23 01.2	83.8559	−5.3837	E	l	near bad column

FITS headers, post-launch shifts in the relative physical locations of the CCDs, and inaccuracies in the geometric mapping from physical locations to angular coordinates. From the two comparisons, it appears that the coordinates listed in Table 4 are accurate to approximately 1 arcsec—quite suitable for our present purposes. At some later date, it should be possible with further processing to obtain positions with accuracies approaching the PC's resolution—such high accuracy would be extremely worthwhile for future proper motion studies. It may be that our Trapezium images could be combined with the astrometric positions of Jones & Walker in order to construct better models of the field and intra-chip effects on position determination for the PC. A detailed discussion of WFPC astrometry is given by D. Monet (1991) in the WFPC Final Orbital/Science Verification Report.

3.3. *Spatial Distribution, Multiple Observations, Visual Binaries*

In Figure 6 we indicate the spatial distribution of the *HST* sample in the inner Trapezium cluster region. The PC stars from Table 4 are shown as open circles with the JW stars indicated as filled circles. As is seen in Table 4, many PC stars are also JW stars.

Slight overlaps between PC fields provided some instances of multiple observations of the same star. These multiple observations are given in Table 5 where we give the individual and adopted V and I magnitudes for each case. In a few instances, an observation falling near the edge of the CCD was considered to be too inaccurate and the other observation was adopted. PC 223 (JW 588) was observed undergoing a flare event during one of its V exposures. The duplicate observations of the fainter component of JW 399 may also indicate the presence of flare activity. Following the adopted magnitudes in Table 5 are the differences in arcseconds between the right ascension and declination positions found for each observation using the xy2rd routine. The remaining columns in Table 5 indicate which PC fields the star falls in, the PC and JW identifications, and additional notes.

The phenomenal scale provided by the PC, $\sim 0''.044$ pixel^{-1},

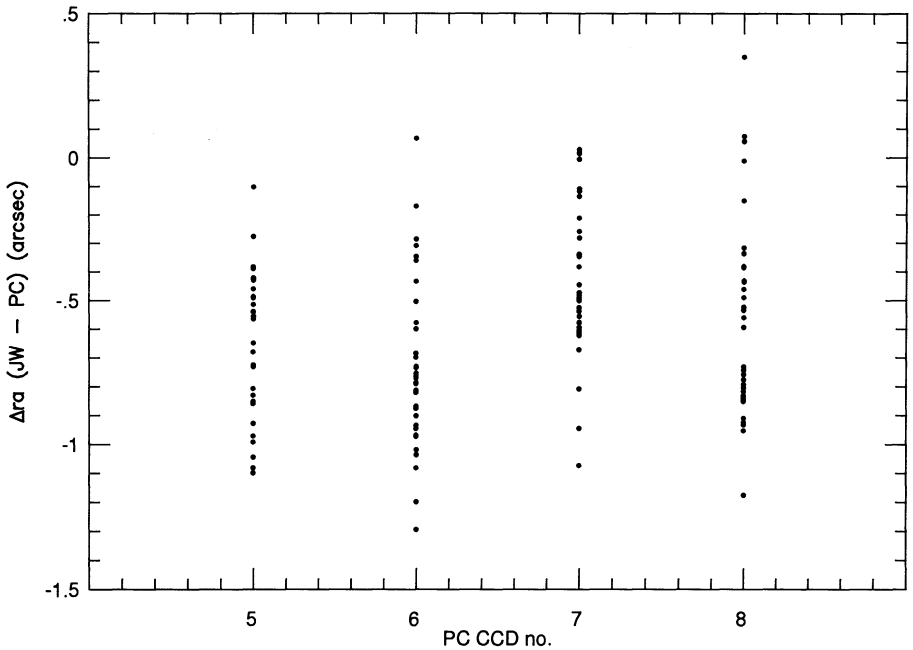

FIG. 4.—Relative differences in α between JW and PC coordinates, plotted vs. CCD chip number

enabled the identification of sub-arcsec separation binaries not previously possible using ground-based images. Table 6 lists those binaries identified, with separations ranging from ~1″.2 (27 pixels) down to ~0″.06 (1.4 pixels). Binary identification was done visually and with the aid of contour mapping and psf fitting to suspected binaries. At a distance of ~440 pc (Warren & Hesser 1978), a separation of 0″.06 corresponds to only 26 AU. (For comparison, the semi-major axis of Neptune's orbit is ~30 AU, while Pluto's distance from the Sun ranges from ~30–40 AU.) The sharp core of the stellar PSF enables fairly easy identification of visual binaries down to ~1 pixel. Binary identification at smaller scales has not been performed here as it requires a more detailed analysis accounting for such influences as telescope jitter on the image shape. As we will discuss in § 4.5, we believe that most of the visual binaries having separations less than 1″ are in fact physical binary systems. In Table 6, we provide for each binary, the PC and JW identifications, the separation between primary and secondary in pixels and arcseconds, the individual *V* and *I* photometry from Table 4 and α and δ positions from the xy2rd routine. Magnitudes were derived for the closest binaries from psf fitting of the central cores. The "model" PSF used was taken in each case

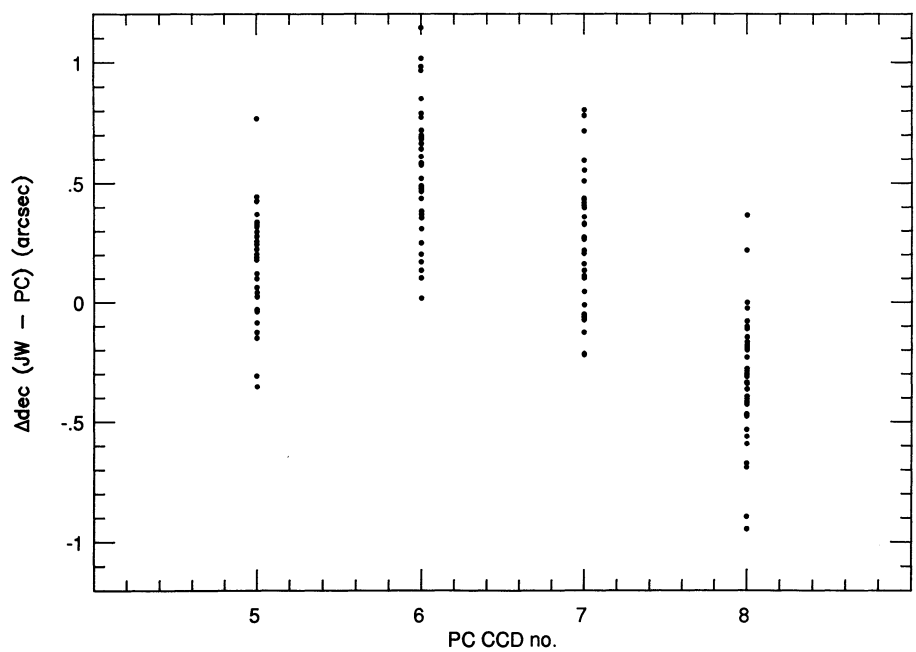

FIG. 5.—Relative differences in δ between JW and PC coordinates, plotted vs. CCD chip number

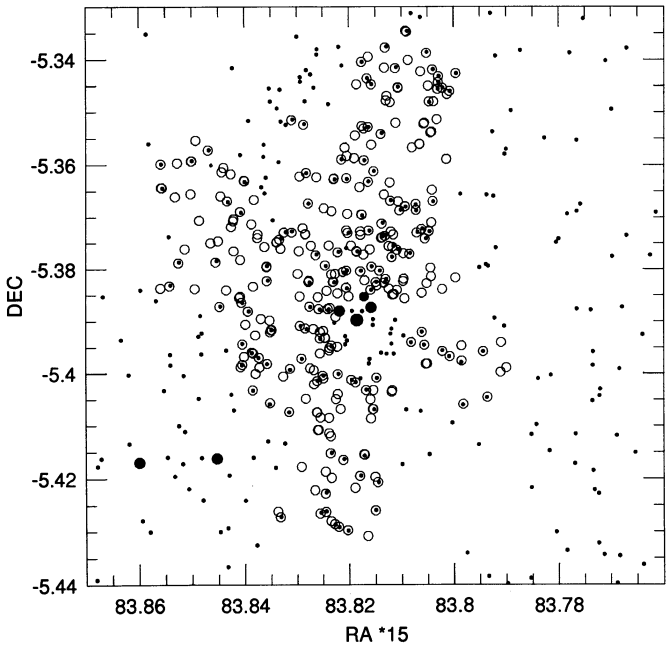

FIG. 6.—Schematic illustration of central Trapezium cluster region, indicating stars observed by *HST*. Open circles correspond to PC stars given in Table 4 and small dots are stars identified in Jones & Walker (1988). Large filled circles are bright stars in the region, shown for orientation.

from either a nearby star of similar magnitude or a single star from another image (using the same filter) falling near the same position as the binary. In cases where there was a large magnitude difference between the components, it was usually difficult to accurately measure the fainter component—in some cases only an *I* magnitude could be measured for the companion. Among the wider binaries, we were able to measure secondaries up to 4 magnitudes fainter than the primary; for separations of ~0.1–0.2 arcsec, the increased background from the primary limited us to secondaries up to ~1.5 magnitudes fainter than the primary. The photometric errors for the close binaries will be higher than the 1 σ values found for similar magnitude single stars, though lacking independent observations, we cannot accurately estimate just what the uncertainties in these binary magnitudes are.

A few stars not listed in Table 6 are worth mention. PC 166 (= JW 539) may be a close binary; it falls too near the edge of the CCD for a definitive determination. JW 562 is resolved in the PC images into the stars PC 200 and PC 194, with a separation of about 1.55 arcsec. The star PC 232 appears to be a very close binary in the PC images; however, one "component" is actually a CCD defect.

3.4. *Additional Photometric Data*

The additional observations of fields B and C with the F413M (*B*) filter did not yield much meaningful information: only about 16 stars with appreciable signal could be measured and the instrumental *B* magnitudes derived could not at this time be transformed into a standard system. We do not tabulate the instrumental *B* magnitudes here, but note that the F413M data confirm JW497 to be redder than other stars of similar *V* magnitude. In Table 7 we note a few *V* magnitudes that could be measured on the 1 second *V* exposure centered on the Trapezium (field A). The *V* photometry in Table 7 was calculated using the same transformation equation (1) as for the other observations.

TABLE 5

MULTIPLE OBSERVATIONS

FLD 1 V	FLD 1 I	FLD 2 V	FLD 2 I	ΔV	ΔI	ADOPTED V	ADOPTED I	ΔRA (″)	ΔDEC (″)	FLDS	PC	JW	NOTES
17.30	14.04	17.72	14.42	−0.42	−0.38	17.49	14.21	0.66	0.47	5 8	29		
19.56	15.55	19.37	15.74	+0.19	−0.19	19.46	15.64	0.69	0.58	8 9	32		FLD 8 near edge (50pix)
19.06	16.02	20.65	16.77	−1.59	−0.75	20.65	16.77	0.61	0.44	5 8	33	399B	cts higher for FLD 5
18.44	15.18	18.51	15.41	−0.07	−0.23	18.48	15.29	0.61	0.44	5 8	34	399A	double
21.29	17.28	22.95	17.48	−1.66	−0.20	22.95	17.48	0.47	0.72	8 9	43		FLD8 near edge,FLD9 V upp.lim.
...	13.04	16.13	13.64	...	−0.60	16.13	13.64	0.43	0.54	5 8	46	411	FLD 5 near edge
18.45	15.21	18.80	15.47	−0.35	−0.26	18.61	15.33	0.58	0.69	5 8	65	442	
22.61	17.72	23.06	17.78	−0.45	−0.06	22.81	17.75	0.53	0.88	8 9	71		FLD 9 near edge (50pix)
19.07	14.93	18.32	14.64	+0.75	+0.29	18.63	14.77	0.28	0.88	8 C	101	473	
17.65	14.70	17.72	14.67	−0.07	+0.03	17.68	14.69	0.10	0.94	8 C	109	481	
...	18.88	...	19.08	...	−0.20	...	18.98	0.35	0.87	8 C	114		
20.56	16.05	20.60	16.17	−0.04	−0.12	20.60	16.17	0.06	0.88	5 6	119		FLD 5 near edge
18.47	14.81	18.57	14.81	−0.10	+0.00	18.52	14.81	0.10	0.86	8 C	121	500	
17.91	14.80	18.27	14.98	−0.36	−0.18	18.08	14.89	0.02	0.21	8 C	131	507	
19.14	14.96	18.99	14.83	+0.15	+0.13	18.99	14.83	0.28	0.06	5 6	132		FLD 5 bad col?
17.11	14.17	17.07	14.14	+0.04	+0.03	17.09	14.15	0.06	0.06	5 6	139	513	
17.31	14.29	17.26	14.39	+0.05	−0.10	17.29	14.34	0.76	0.92	1 2	141	516	
20.28	16.06	20.35	16.03	−0.07	+0.03	20.32	16.05	0.05	0.83	8 C	142		
18.61	14.52	18.65	14.59	−0.04	−0.07	18.63	14.55	0.72	1.15	1 2	168	540	
18.80	14.66	18.93	14.72	−0.13	−0.06	18.86	14.69	0.78	1.20	1 2	193	559	
17.90	14.30	18.02	14.35	−0.12	−0.05	17.90	14.30	0.50	0.45	2 4	212	575	FLD 4 near edge
19.46	15.92	17.95	15.77	+1.51	+0.15	19.46	15.92	0.53	0.42	2 4	223	588	V Flare, FLD 4 near edge
17.01	13.86	17.10	13.96	−0.09	−0.10	17.05	13.91	0.56	1.08	2 4	228		
20.28	15.50	20.50	15.66	−0.22	−0.16	20.39	15.58	0.01	0.49	2 4	238		
15.74	13.01	15.43	12.98	+0.31	+0.03	15.43	12.98	0.13	0.48	2 4	254	622	FLD 2 near edge
21.81	16.85	22.62:	16.95	−0.81 :	−0.10	21.81	16.85	0.09	0.20	6 7	261		FLD 7 near edge
19.82	16.14	19.78	16.10	+0.04	+0.04	19.80	16.12	0.09	0.55	6 7	269	657	
18.82	15.17	19.04	15.32	−0.22	−0.15	19.04	15.32	0.12	0.01	6 7	280		FLD 6 near edge
19.79	15.18	19.76	15.26	+0.03	−0.08	19.78	15.22	0.06	0.04	4 7	284	685	FLD 4 near edge
20.28	16.66	...	...	...	...	20.28	16.66	0.38	1.40	B 7	298		both near edge

TABLE 6

VISUAL BINARIES

PC	JW	SEPARATION (pixels)	(″)	PRIMARY V	I	V−I	COMPANION V	I	V−I	PRIMARY RA	DEC	COMPANION RA	DEC	NOTES
11/12	378	2.28	0.10	15.00	12.89	2.11	15.81	13.49	2.32	5:35:12.170	-5:23:48.15	5:35:12.172	-5:23:48.25	
13/14	377	1.93	0.08	19.57	15.30	4.27	20.96	16.31	4.65	5:35:12.194	-5:20:45.67	5:35:12.199	-5:20:45.69	
16/17		4.56	0.20	22.20	19.05	3.15	21.98	19.63	2.35	5:35:12.333	-5:21:32.16	5:35:12.334	-5:21:31.96	16/17 V upp.lim.
34/33	399	5.28	0.23	18.44	15.18	3.27	19.06	16.02	3.04	5:35:13.138	-5:22:21.85	5:35:13.135	-5:22:21.62	
	399	5.30	0.23	18.51	15.41	3.10	20.65	16.77	3.88	5:35:13.097	-5:22:21.41	5:35:13.094	-5:22:21.18	
37/40		21.25	0.93	21.03	17.26	3.78	22.38	17.68	4.70	5:35:13.212	-5:23:53.18	5:35:13.274	-5:23:53.30	37/40 V upp.lim.
48/49		6.71	0.29	19.69	16.27	3.42	20.11	17.89	2.22	5:35:13.563	-5:21:21.91	5:35:13.578	-5:21:21.71	
57/58	435	20.68	0.91	19.30	15.70	3.61	...	19.20	...	5:35:14.172	-5:20:05.07	5:35:14.218	-5:20:04.48	
59/60	436	6.94	0.30	20.93	17.52	3.41	21.31	16.97	4.34	5:35:14.229	-5:22:04.54	5:35:14.247	-5:22:04.38	
68/67	445	10.26	0.45	18.92	14.67	4.24	21.68	16.03	5.65	5:35:14.576	-5:20:42.90	5:35:14.570	-5:20:43.34	
73/75		23.03	1.01	20.14	17.83	2.31	21.20	16.38	4.82	5:35:14.744	-5:23:05.30	5:35:14.809	-5:23:05.59	
'80'/77		27.25	1.20	17.59	14.26	3.32	18.18	14.40	3.78	5:35:14.853	-5:24:12.74	5:35:14.824	-5:24:11.62	'80'=80/79
80/79		1.44	0.06	18.14	14.86	3.27	18.60	15.29	3.30	5:35:14.855	-5:24:12.76	5:35:14.851	-5:24:12.73	
99/98	472	1.98	0.09	18.12	14.84	3.28	18.44	15.08	3.36	5:35:15.331	-5:22:26.33	5:35:15.330	-5:22:26.25	
111/112	484	9.06	0.40	18.96	15.78	3.18	22.79	16.88	5.92	5:35:15.695	-5:24:24.71	5:35:15.721	-5:24:24.66	
126/125	504	1.55	0.07	15.83	13.64	2.19	15.98	13.57	2.41	5:35:15.989	-5:20:36.87	5:35:15.990	-5:20:36.80	
129/130	509	12.04	0.53	18.48	15.06	3.42	19.31	15.67	3.64	5:35:16.092	-5:24:55.89	5:35:16.118	-5:24:55.53	
136/134	511	9.67	0.42	19.47	15.67	3.80	...	17.98	...	5:35:16.229	-5:22:10.03	5:35:16.206	-5:22:10.28	
144/143	519	8.76	0.38	17.77	14.30	3.47	19.87	17.51	2.36	5:35:16.447	-5:22:35.47	5:35:16.438	-5:22:35.83	
152/150	526	3.05	0.13	13.77	11.87	1.90	15.58	13.40	2.18	5:35:16.697	-5:24:04.50	5:35:16.694	-5:24:04.38	
173/172	551	3.22	0.14	16.60	13.87	2.73	16.92	14.36	2.56	5:35:17.293	-5:25:44.67	5:35:17.283	-5:25:44.66	
183/184	552	10.62	0.47	17.15	14.50	2.65	19.21	15.96	3.25	5:35:17.486	-5:21:45.30	5:35:17.499	-5:21:45.73	
185/186	553	8.46	0.37	14.91	12.41	2.49	16.85	14.93	1.91	5:35:17.504	-5:22:56.66	5:35:17.527	-5:22:56.80	
202/203	570	3.63	0.16	17.85	14.73	3.12	18.81	15.28	3.53	5:35:17.868	-5:25:34.60	5:35:17.868	-5:25:34.44	
208/206		2.88	0.13	20.12	15.93	4.20	20.93	16.18	4.75	5:35:17.893	-5:23:35.30	5:35:17.888	-5:23:35.40	
219/221		15.24	0.67	19.63	16.19	3.43	20.61	16.72	3.89	5:35:18.190	-5:24:38.94	5:35:18.235	-5:24:39.00	
224/222		9.67	0.42	19.11	15.16	3.94	19.97	16.13	3.84	5:35:18.285	-5:24:26.83	5:35:18.258	-5:24:26.94	
235/234	598	20.80	0.91	15.75	13.05	2.71	...	16.69	...	5:35:18.651	-5:22:56.74	5:35:18.629	-5:22:55.89	
241/239		5.43	0.24	20.31	16.77	3.54	...	17.54	...	5:35:18.809	-5:22:23.78	5:35:18.797	-5:22:23.61	
263/262	648	15.27	0.67	15.73	13.15	2.58	19.09	14.62	4.47	5:35:20.392	-5:23:30.16	5:35:20.348	-5:23:30.04	
282/279	681	25.34	1.11	16.26	13.86	2.40	20.38	16.39	3.99	5:35:21.258	-5:23:45.49	5:35:21.198	-5:23:46.15	
288/286	687	11.26	0.49	17.67	14.66	3.00	...	17.32	...	5:35:21.623	-5:21:46.74	5:35:21.596	-5:21:47.03	
294/296		25.77	1.13	21.54	17.09	4.45	23.76	19.40	4.36	5:35:21.789	-5:23:06.90	5:35:21.839	-5:23:07.76	296 V upp.lim.
315/314	748	8.40	0.37	17.91	14.77	3.14	20.62	16.01	4.62	5:35:24.034	-5:21:33.36	5:35:24.009	-5:21:33.31	
322/321	766	2.52	0.11	16.37	13.64	2.73	16.86	13.87	2.98	5:35:25.008	-5:22:59.59	5:35:25.001	-5:22:59.57	
323/324	776	11.67	0.51	16.71	14.20	2.52	19.77	15.85	3.92	5:35:25.353	-5:21:51.71	5:35:25.386	-5:21:51.56	

4. DISCUSSION

4.1. *Comparison to HT*

In Table 8 we list the 61 stars observed by *HST* that are in common with the sample observed by HT. The (V, I_C) photometry from *HST* and HT are given, followed by the difference (*HST* − HT) between them, identifications (JW, HT, PC), and notes. In a few instances, bright stars observed by HT were not always measurable by *HST* in both V and I (i.e., Par 1885 = JW 531) due to CCD saturation. Figures 7 and 8 illustrate the differences in V and I_C as a function of magnitude. Resolved binaries in the *HST* sample and stars denoted as variable by JW are indicated. Large magnitude differences between the *HST* and HT samples are seen to be primarily attributable either to the resolution of close binaries by *HST* or inherent variability amongst the stars.

TABLE 7

ADDITIONAL V MAGNITUDES (FIELD A)

Star	V	V From Table 4	0ther
P1864	10.31	...	
P1892	10.18	...	
JW480	14.83	14.51	PC105
JW499	13.12	...	
JW503	15.50	...	
JW515	14.35	...	
JW526	14.46	13.77	PC152
JW538	13.39	...	
JW581	14.52	13.92	PC216

JW 497 and 562 may also be variable or else the HT photometry for these is inaccurate. Subsequent to producing Table 8 and Figures 7 and 8, we discovered that the stars A24 and A121 of HT correspond to PC 228 and PC 256, respectively. Also, A124 and A125 as listed in Table 1 of HT could not be precisely identified in the present study; however, their magnitudes and relative positions as given by HT suggest that they may correspond to JW 766 and JW 782. The conversion formulae relating instrumental and calibrated magnitudes are not significantly changed by inclusion or exclusion of these stars.

4.2. *V, V − I Diagram*

In Figure 9 we plot the *HST* photometry from Table 4; several stars observed by *HST* but without V magnitudes or

TABLE 8

HERBIG-TERNDRUP (HT) STARS IN COMMON

HST V	HST I_C	HT V	HT I_C	HST − HT ΔV	HST − HT ΔI	JW	HT	PC	NOTES
12.46	10.36	12.36	10.31	+0.10	+0.05	352	P1784	5	
15.00	12.89	14.23	12.18	+0.77	+0.71	378	P1808	11	double
12.64	11.02	12.82	11.13	−0.18	−0.11	385	P1807	19	
...	12.49	14.63	12.97	...	−0.48	391	P1806	23	
14.46	12.55	15.09	12.88	−0.63	−0.33	409	P1824	42	poor V match
16.13	13.54	16.29	13.50	−0.16	+0.04	411	P1820	46	
16.86	13.60	16.84	13.67	+0.02	−0.07	420	P1821	50	
14.40	12.30	14.44	12.30	−0.04	+0.00	423	P1819	51	
15.28	12.51	15.22	12.44	+0.06	+0.07	431	P1823	54	
16.30	13.04	16.32	13.16	−0.02	−0.12	432	P1822	55	
14.58	12.10	14.69	12.20	−0.11	−0.10	448	P1839	70	
13.96	11.86	13.95	11.91	+0.01	−0.05	454	P1840	78	
14.49	12.53	...	12.32	...	+0.21	457	P1837	82	
14.26	12.12	...	12.14	...	−0.02	463	P1841	89	
15.21	13.06	15.29	13.19	−0.08	−0.13	467	P1838	91	
13.16	11.50	13.22	11.45	−0.06	+0.05	468	P1842	94	
15.17	12.54	15.56	12.78	−0.39	−0.24	470	A7	97	
16.04	13.34	16.27	13.24	−0.23	+0.10	476	P1861	102	poor fit
13.83	11.55	...	11.64	...	−0.09	478	P1872	103	
12.77	10.97	12.99	11.06	−0.22	−0.09	479	P1862	106	
14.51	12.44	14.52	12.48	−0.01	−0.04	480	P1871	105	
17.68	14.69	...	14.75	...	−0.06	481	A2	109	
17.11	13.83	...	13.64	...	+0.19	492	P1860	113	
17.01	14.24	...	14.00	...	+0.24	496	A8	120	
17.07	13.63	16.04	13.56	+1.03	+0.07	497	A4	123	good I match, poor V
18.52	14.81	...	14.85	...	−0.04	500	A1	121	
15.83	13.64	...	12.82	...	+0.82	504	P1859	125	double
18.08	14.89	...	15.28	...	−0.39	507	A3	131	
18.48	15.06	...	14.68	...	+0.38	509	A201	129	double
17.29	14.34	...	14.17	...	+0.17	516	A109	141	
13.77	11.87	13.63	11.67	+0.14	+0.20	526	P1896	150	double
14.90	12.40	14.86	12.47	+0.04	−0.07	529	P1886	154	
...	9.99	10.47	9.86	...	+0.13	531	P1885	159	
15.06	12.62	14.85	12.50	+0.21	+0.12	533	P1888	161	
18.63	14.55	...	14.85	...	−0.30	540	A113	168	
13.04	10.82	13.03	10.94	+0.01	−0.12	544	P1884	170	
16.29	13.91	14.74	12.57	+1.55	+1.34	548	P1909	174	known variable
17.15	14.50	15.70	13.52	+1.45	+0.98	552	P1908	183	resolved double
14.91	12.41	14.72	12.35	+0.19	+0.06	553	P1911	185	double
18.86	14.69	...	14.96	...	−0.27	559	A114	193	
15.68	13.01	...	14.30	...	−1.29	562	P1912	200	bad H&T phot?
11.39	9.66	12.01	10.11	−0.62	−0.45	567	P1910	207	bright, near edge
17.90	14.30	...	14.55	...	−0.25	575	A134	212	
13.92	11.58	13.93	11.76	−0.01	−0.18	581	P1913	216	
13.42	11.30	13.38	11.33	+0.04	−0.03	589	P1925	226	
15.58	13.06	15.70	13.35	−0.12	−0.29	596	P1927	233	variable, ft. on HST
15.75	13.05	15.78	13.28	−0.03	−0.23	598	P1926	234	visual binary 1″
17.45	14.22	...	14.26	...	−0.04	600	A115	236	
15.63	13.42	15.64	13.33	−0.01	+0.09	603	P1924	237	
17.01	13.68	...	13.70	...	−0.02	606	A6	242	
15.50	13.64	15.26	13.44	+0.24	+0.20	607	A10	244	
16.59	13.89	16.65	13.91	−0.06	−0.02	610	P1928	247	
17.00	14.41	...	14.34	...	+0.07	620	A25	253	
15.35	12.89	15.27	12.80	+0.08	+0.09	622	P1940	254	
15.73	13.15	15.43	13.04	+0.30	+0.11	648	P1960	262	double
18.18	14.03	...	14.46	...	−0.43	659	A30	267	
12.43	10.76	12.25	10.68	+0.18	+0.08	669	P1961	273	
16.86	14.48	16.79	14.20	+0.07	+0.28	679	P1991	281	
16.26	13.86	15.93	14.16	+0.33	−0.30	681	A31	282	poor fit, visual binary 1″
13.27	11.83	13.40	11.82	−0.13	+0.01	698	P1973	290	
17.89	14.72	...	14.61	...	+0.11	723	A130	306	

only having upper limits in V are not plotted. The *HST* data are believed to be complete down to $V \simeq 20$. The reddening vector $A_V = 2.9E_{V-I}$ and the mean cluster reddening of 0.84 (HT) is shown. The figure shows that we have accomplished the primary observational goal of the project—the new color-magnitude diagram extends at least 5 magnitudes fainter than HT's photometry.

Five stars in the region observed by *HST* are proper motion nonmembers of the Trapezium according to JW. Two of these (JW 349 and JW 583) fall well below the locus of Trapezium members in Figure 8, and we assume that they are indeed field main-sequence dwarfs slightly foreground to Orion. The other three stars (JW 494, JW 496, and JW 532) fall within the main locus of Trapezium stars in Figure 9 and we consider their membership status uncertain. JW 494 and JW 532 are deeply embedded in nebulosity which could have adversely affected their measurement for proper motions. While not as deeply embedded as the other two, JW 496 may also have been simi-

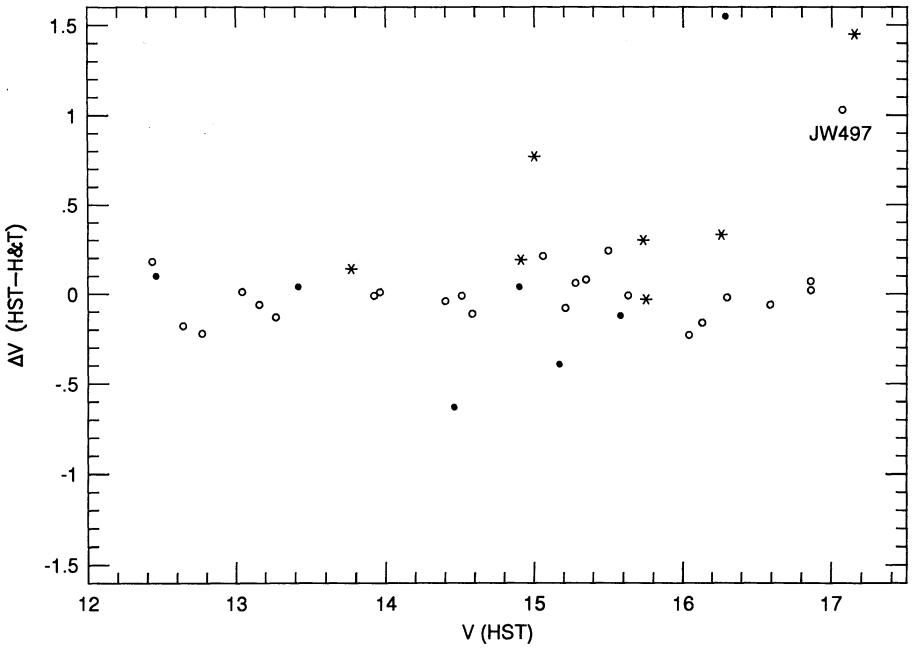

FIG. 7.—Comparison of *V* magnitudes for 61 stars in common with HT (Table 8). Binaries resolved by *HST* are plotted as asterisks (*) and filled circles indicate stars noted as variable by JW.

larly affected by the surrounding nebulosity. (JW 349 and JW 583 are further away from the core nebulosity region and their proper motion measurement may therefore be more reliable.) Two nonstellar objects are seen to fall below the cluster sequence; these objects will be discussed in more detail later. (JW 532 is also associated with a nonstellar or nebulous appearance in the PC frames.) No proper motion information is available for the other stars (PC 118, 189, and 260) which fall well below the main locus of Trapezium members.

Three secondary components of binary systems also lie significantly below the cluster sequence; JW 553b (= PC 186) and JW 519b (= PC 143) are components of similar visual binary systems (Table 6) which have a *V* magnitude difference between primary and companion of ~2 mag and separations of ~0.37 arcsec, and the other binary component, PC 49, is separated about 0.29 arcsec from the primary, with a small magnitude difference between the primary and secondary. We are puzzled by the photometric properties of these stars, simply because we find no fully satisfactory explanation for them. One might assume that their photometry is inaccurate due to the

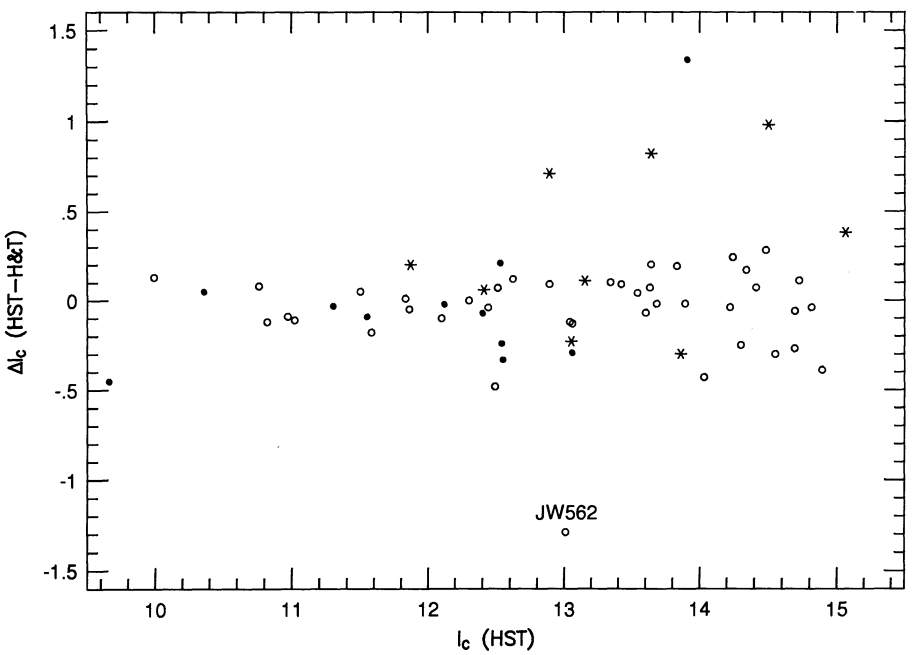

FIG. 8.—Same as Fig. 7, but for *I* magnitudes. Symbols are the same as in Fig. 7

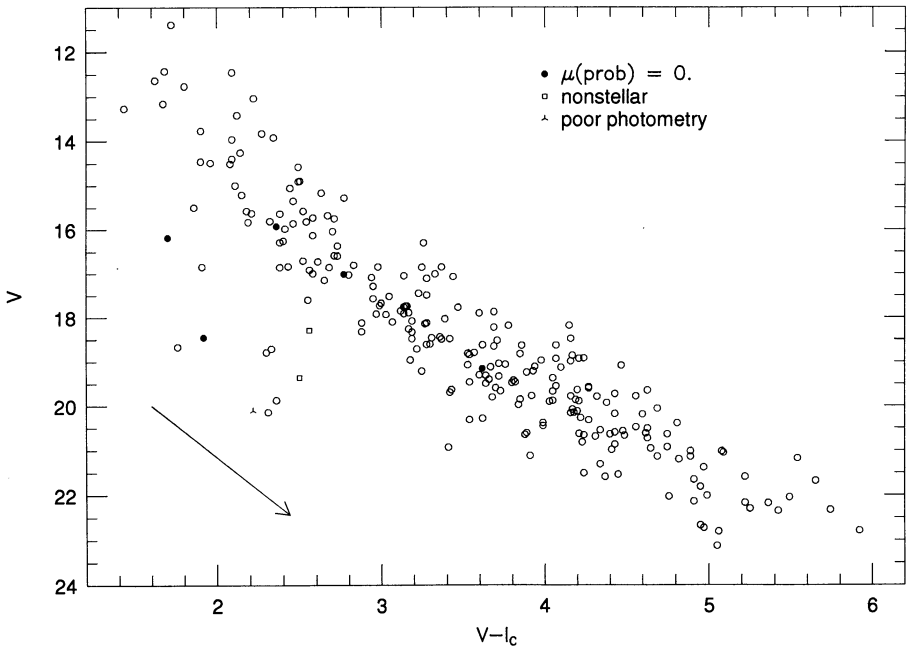

FIG. 9.—Color-magnitude diagram for all stars observed by *HST* and with (V, $V-I$) photometry. Stars with upper limits in V are not plotted. The reddening vector for $A_V = 2.9E(V-I)$ and a mean reddening of 0.84 (Herbig & Terndrup 1986) is shown.

influence of the primary's light. We have carefully rechecked the analysis, however, and do not believe that this is the case. One might imagine that there is some physical interaction between the primary and secondary that is causing the secondary to have peculiar colors, but at separations greater than 100 AU we believe this to be unlikely. That the blue secondaries' exist is due to flare events during the V filter exposures is possible, but an unlikely one we believe. Other possible explanations seem incompatible with the statistics of our observations: about one-tenth of our stars are visual binaries, and about one-tenth of those binaries have peculiar photometric properties (i.e., the stars have V and $V-I$ photometry that places them on or near the ZAMS—and therefore lie below the general cluster locus). If the factor which causes these secondares to have this system is not intrinsic to their being in a binary, then the nonbinary population should have a similar fraction of stars exhibiting the same symptom—on the order of $0.1 \times 249 \simeq 25$ nonbinary stars should fall on or near the ZAMS and below the cluster locus, instead of the approximately 7–8 such stars we see.

To better compare our results to HT's previous study, we plot in Figure 10 all those HT stars having V, $V-I_C$ photometry together with the *HST* photometry from Figure 9, but now excluding the nonstellar objects and proper motion nonmembers. To facilitate comparison with HT's Figure 2, we plot the same evolutionary isochrones (1, 4, 10×10^6 yr, 3.0–0.7 $M_\odot$) from published work of VandenBerg (1984) that were also used by HT in their analysis. Perhaps the most informative feature of Figure 10 is that the widths in the cluster sequence revealed by the HT and *HST* data are consistent over the magnitude range in common, and that the width of the general cluster sequence as revealed by the new data appears to remain essentially unchanged down to at least $V \simeq 20$.

In Figure 11 we show the *HST* data from Figure 10 along with only those HT stars not observed by *HST*. To aid in interpretation, we plot several additional items. The lower envelope to the Pleiades cluster (Stauffer & Hartmann 1987) has been combined with the observational zero-age main sequence (ZAMS) from Stauffer & Hartmann (1986) to form an observational ZAMS at the Trapezium's distance and reddening. [An apparant distance modulus of $(m-M) = 10.62$ and reddening of $E(V-I)_C = 0.84$ have been used here.] The observed M dwarf main sequence as found by Bessel (1991) and the theoretical ZAMS from the 1.0–0.3 $M_\odot$ evolutionary tracks of VandenBerg (1987) are also indicated. New model calculations by Fritz Swenson (Swenson et al. 1994, hereafter FJS) for the range 5.0–0.15 $M_\odot$ were kindly provided to us in advance of publication. FJS's evolutionary tracks are computed using his own evolutionary code employing new opacities (both interior and surface), having the degenerate Debye-Hückel correction in the equation of state, and using bolometric correction determinations described in VandenBerg (1992). FJS's calculations employ the most up-to-date physics and in fact the FJS ZAMS in Figure 11 is in better agreement than previous calculations with the observed ZAMSs of Stauffer & Hartmann, and Bessel. From FJS's models, we plot the isochrones for 1, 4, and 10×10^6 yr over the mass range 5.0–0.15 $M_\odot$ in Figure 11. An expanded view of some of the Trapezium photometry is given in Figure 12, with most of the same information as in Figure 11 and the addition of the evolutionary tracks corresponding to 1.5, 1.0, 0.6, and 0.5 $M_\odot$. It is clear from examination of Figures 11 and 12 that considerably more than 50% of the Trapezium stars have ages less than 10^6 yr.[2]

Because the Trapezium stars are quite young, their surface gravities are expected to be intermediate between that of main-sequence stars and giants. Standard color-temperature conver-

[2] For low masses ($\lesssim 0.4\ M_\odot$, or $V-I_C > 2.8$), the isochrones shown in Fig. 11 should be considered as particularly uncertain due to the incomplete treatment of molecular opacities and the difficulties attendant with converting from the theoretical (M_{bol}, log T_{eff}) to the observational (V, $V-I$) plane.

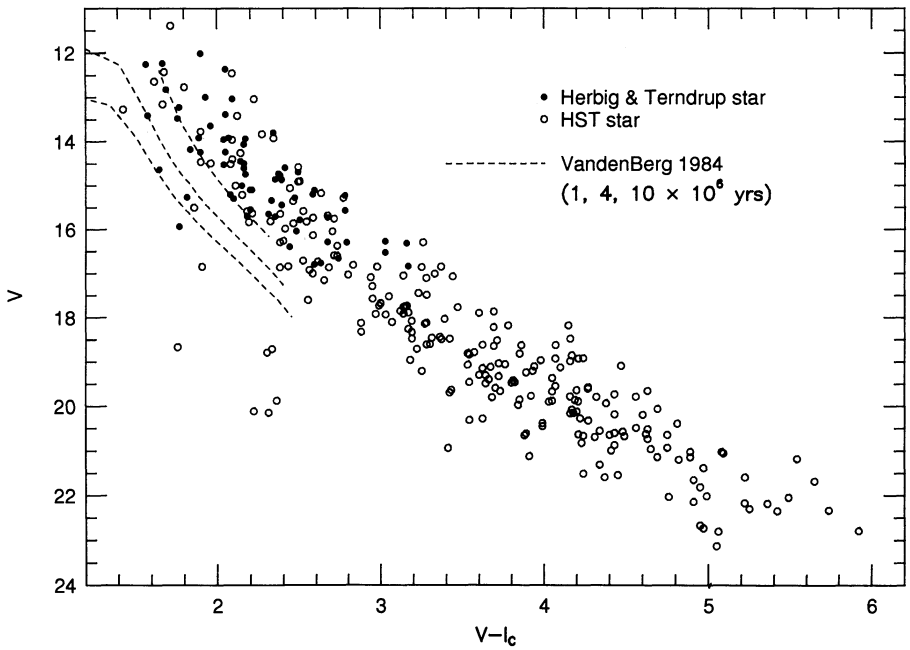

FIG. 10.—V vs. $V-I$ diagram showing HT stars together with *HST* photometry from Fig. 9. Nonstellar objects and proper motion nonmembers have been excluded. The isochrones from VandenBerg (1984) are indicated.

sions may therefore be inaccurate. Using the FJS models as a guide, the surface gravities for our Trapezium cluster stars are closer to that of dwarfs than of giants, which is why we used a color-temperature conversion appropriate for dwarfs. A conversion relation appropriate to subgiants would be better, but none exists as far as we are aware. [The color-temperature conversion for giants (Bessell 1979) is so significantly different at cool temperatures from that of dwarfs that it leads to considerable uncertainty in placement of the theoretical tracks if one tries some combination of dwarf and giant color-temperature conversions.] A brief discussion of the various color-temperature relations is given in the Appendix.

In comparing Figures 11 and 12 to Figure 10, one may notice a difference in the appearance of certain stars falling below the general cluster sequence. Thus, JW 391, 607, and 681 (all proper motion members by JW) fall noticeably below the

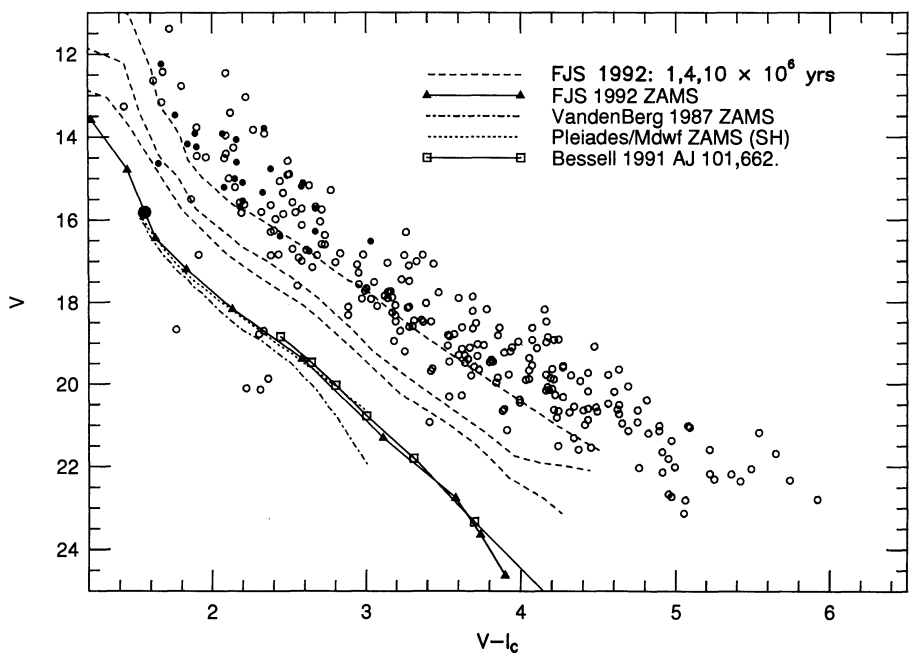

FIG. 11.—V vs. $V-I$ diagram similar to Fig. 9, but now showing only those HT stars which were not observed by *HST*. In addition to other observational and theoretical ZAMS relations described in the text, theoretical evolutionary models by F. Swenson (FJS) are shown. The FJS age isochrones are plotted down to 0.15 $M_{\odot}$, while the FJS ZAMS is indicated down to 0.2 $M_{\odot}$. The location on the ZAMS of 1 $M_{\odot}$ is indicated with a large filled circle. One interesting feature of the new observations is that spread or width of the general cluster sequence appears to remain essentially the same over the magnitude range covered.

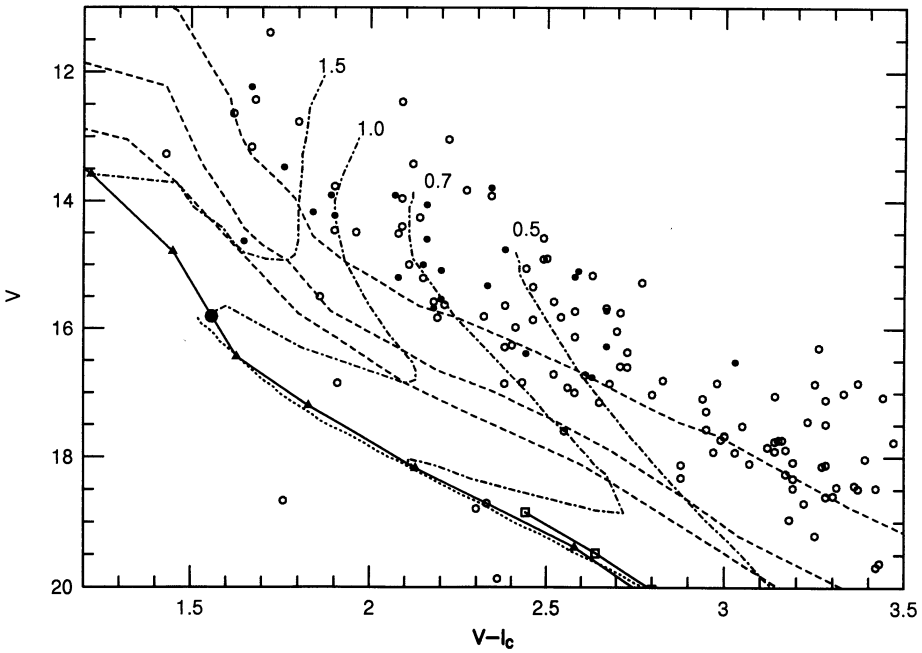

FIG. 12.—Expanded view of Fig. 11, with evolutionary tracks for certain masses plotted

cluster sequence as observed by HT in Figure 10. In Figures 11 and 12 however, only JW 607 and JW 391 are shown as falling below the cluster sequence. What has happened to JW 681? The *HST* photometry of JW 681 (V, $V-I = 16.26, 2.40$) places the star at a redder color than HT's photometry—placing it among the general cluster sequence of stars in Figures 11 and 12. JW 391 was observed by *HST*, though only an I magnitude could be measured. It is plotted in Figures 11 and 12 using the HT (V, $V-I$) values. While no reliable *HST* V magnitude could be measured, JW 391 is almost 0.5 magnitudes brighter in I_C as observed by *HST* compared to HT; suggesting that JW 391 may normally be redder than as observed by HT.

4.3. *Age and Age Spread*

The unambiguous detection of a range of formation times or "age spread" amongst a cluster or association of stars would open new observational avenues of study in the area of star formation research. Because pre–main-sequence isochrones lie closer together as one goes to older ages, the reliable detection of an age spread is likely to be most conclusively established in a relatively young cluster. Many attempts to make this type of measurement have been done before (Iben & Talbot 1966; Adams, Strom, & Strom 1983; Stahler 1985; Cohen & Kuhi 1979), but with somewhat mixed results. The Trapezium cluster many be the ideal cluster for such a detection; it is not not only very young, but also very populous. In Figure 12, at a given color the separation between the lower envelope and upper envelope of the cluster sequence is typically on the order of two magnitudes. As we have seen, the width of the general cluster sequence appears generally consistent over the range sample by *HST*. How is this width to be interpreted? Possible contributors to the observed spread include:

1. *Duplicity*:—The presence of binary companions will result in a fraction of the stars in any cluster to lie above the locus for single stars. The maximum vertical displacement in a color-magnitude diagram, which occurs in the case of an equal-mass binary, is 0.75 magnitudes. Since the typical range in V at a fixed $V-I$ for the Trapezium cluster stars is approximately 2 magnitudes, unresolved binaries do not appear to be the primary contributor to this observed spread.

2. *Photometric errors*.—This however, is unlikely to be a significant contributor at the bright end ($V \leq 18$) since our V and I magnitudes are accurate to less than 0.1 mag. With these errors, we would predict a one-sigma error in $V-I$ of ~ 0.15 mag. The slope of the Trapezium cluster locus of Figure 9, $dV/d(V-I)$, is ~ 2.4, so a 0.15 mag error in $V-I$ would lead to a vertical displacement of ~ 0.35 mag, which is small in relation to the total 2 mag spread.

3. *Differential reddening*.—If the reddening is not parallel to the slope of the cluster locus and if the stars we have observed have greatly differing A_Vs, then a significant portion of the vertical spread in Figure 9 could be due to differential reddening. We expect to place limits on this effect by combining our optical photometry with near-IR photometry and with spectroscopy of a sample of our stars.

Lacking, at present, any new reddening data, we must limit ourselves to noting how reddening might affect our ability to place limits on the time-spread of star formation in the Trapezium: (*a*) If the reddening vector is essentially parallel to the cluster locus, then differential reddening has no effect on our ability to measure an age spread; (*b*) If the reddening vector is shallower than the cluster locus, then differential reddening will spread stars to younger ages. From examination of Figure 11, this effectively means we cannot say anything about the age distribution for ages $\leq 10^6$ yr. We do not consider that to be a severe impediment, since our primary interest is in determining whether there is any evidence for a time-spread of star formation of order 10^7 yr (i.e., long compared to the sound speed crossing time of the protocluster); (*c*) If the reddening vector is steeper than the cluster locus, then differential reddening will scatter younger stars below the 10^6 yr isochrone, making it appear as if the star formation extended over a longer time period than was actually the case. This, along with the errors in our photometry, and the possible presence of a few foreground

dwarfs in our CM diagram acts to make our estimate of the number of "old" ($\geq 10^6$ yr) stars an upper limit. These limitations are acceptable for our present purposes.

It is useful to consider how mass segregation might affect our interpretation of these matters. The fact that the θ^1 Ori stars are well concentrated to the center of the cluster (Zinnecker et al. 1992), suggests that some mass segregation has taken place. In the blister model of the H II region, θ^1 Ori, and other high-mass stars, lie at the center of a hole in the front edge of the molecular cloud—and thus would be expected to have relatively little reddening. If the low-mass stars were not wholly contained in the blister area, but extended into the molecular cloud, then we would see a considerable amount of differential reddening among these stars. If differential reddening were the primary cause for the observed ~ 2 mag spread in V, we would then predict a larger spread for the low-mass stars than for the high-mass stars—which is contrary to what we see. We consider this as one bit of evidence that differential reddening is not the primary contributor to the ~ 2 mag spread. We do note, however, that the range in mass over which our data are complete is only about a factor of 4, and the cluster is probably only a few crossing times old, so mass segregation in our sample is not likely to be a large effect.

It is very probably true that if there was a significant time-spread of star formation in the Trapezium, then the older stars, which might primarily be low-mass stars (Herbig 1982), are likely from dynamical evolution to have a more dispersed radial distribution than the younger stars. The fact that our *HST* fields are concentrated near θ^1 Ori and that stars too far from θ^1 Ori might be so heavily extincted as to be undetectable by us biases us against including the relatively older stars. We suspect, but cannot prove, that this is not a large effect.

4. *Disks.*—As these are very young stars, the presence of circumstellar disks may affect their observed magnitudes and colors. The size and influence of this effect depends on the particular viewing angle relative to the disk, the disk thickness and accretion rate, the grain scattering properties, etc. (Strom et al. 1989; Kenyon & Hartmann 1990; Kroupa, Gilmore, & Trout 1992). Infrared photometry of the Trapezium stars should aid in determining if disks are present for these stars, and if so, to what degree their presence affects the photometry here.

5. *Age spread.*—The remaining probable contributor to the ~ 2 mag spread in the color-magnitude diagram is an age spread. Given the above caveats, and given the normal caveats concerning the reliability of age estimates from use of theoretical isochrones, we can use our observations to place limits on the age spread of the Trapezium stars. To do this, we have simply counted stars in the age ranges indicated by the isochrones in Figure 11. The result of this exercise is that 80% of the stars have estimated ages less than 1 Myr, 15% have ages between 1 to 4 Myr, 2% have ages between 4 and 10 Myr, and 3% have positions in the CM diagram which place them on or below the ZAMS. We suspect that most of the latter stars are either nonmembers or are stars whose colors have either been mismeasured or are affected by circumstellar disks (as in the case of the star Walker 90 in NGC 2264; Strom, Strom, & Yost 1971). The bottom line is that star formation in the Trapezium cluster appears to have been remarkably coeval, and that only a small fraction of the stars may (if truly members) have been born outside of a 1 Myr era of star formation. Because there are other possible contributors to the observed dispersion in the CM diagram, we have more likely overestimated the age spread than underestimated it.

We note that this result is particularly important when considering the topic of the rotational velocities and lithium abundances of low-mass stars in young open clusters. We (Stauffer & Hartmann 1986; Balachandran, Lambert, & Stauffer 1988; Prosser 1992; Soderblom et al. 1993) have shown that there is a large spread in the rotational velocities and lithium abundances for low-mass stars in open clusters with ages ≤ 100 Myr. One possible explanation for these results was that these clusters had significant age spreads among their low-mass stars—at least about one-third of the stars had to be $\geq 10^7$ yr older than the other cluster members if this was correct. If we take the Trapezium cluster result as a guide, this type of explanation for the rotational velocity and lithium data is excluded because the allowed age spread is too small ($\ll 10^7$ yr).

4.4. *Observed Luminosity Function*

The large and highly variable reddening which we expect to be encountered in the Trapezium cluster necessitates the use of additional observations (e.g., near-infrared photometry, spectra) in order to deredden cluster members and derive a reliable, true luminosity (or mass) function as opposed to the directly observed apparent luminosity function. We do not have enough additional data yet in order to significantly improve on the mean cluster reddening estimate by HT, so for now we present only the apparent luminosity function. This is primarily useful for determining whether we see a turnover in the star counts prior to reaching our completeness limit.

In Figure 13 we show the $M(V)$ and $M(I_C)$ luminosity functions of the *HST* PC stars from Table 4. A mean reddening of $E(V-I)_C = 0.84$ ($A_V = 2.4$) and a distance of 440 pc have been assumed to yield $(m - M)_V = 10.62$. With these values for $E(V-I)$ and A_V, then $A_I \simeq 1.56$ and $(m - M)_I = 9.78$.[3] Two stars not observed by us, JW 515 and JW 536, were included in Figure 13 because they fell within the confines of the PC images, yet were not recorded (JW 515 falling between chips, JW 536 falling on a bad column). The luminosity functions are seen to be steeply rising until peaking at around $M_V \sim 9$ ($V \simeq 20$) and $M_I \sim 7$ ($I \simeq 17$). The more precipitous fall-off in N_V past $M_V \simeq 9$ is due to the increasing incompleteness of the data in V at these magnitudes. While our completeness limit in V corresponds to $V \sim 20$ and hence to the peak seen at $M_V \sim 9$, our completeness limit in I_C is ~ 19 and corresponds to the region beyond the $M_I \simeq 7$–8 peak in Figure 13.

According to the FJS models, the corresponding masses at which the V and I luminosity functions appear to peak are $\sim 0.2\ M_\odot$ for $V \sim 20$, and ~ 0.2–$0.15\ M_\odot$ for $I \sim 17$. If our simple mean reddening correction is approximately valid for all the stars we have observed, then it would appear that the lowest mass stars reached in V are on the order of $\sim 0.15\ M_\odot$ (Fig. 11). Preliminary analysis of the optical and infrared photometry for the PC stars reveals however that most stars with $V \geq 20.5$ are highly reddened and the lowest mass stars reached in V may therefore be more on the order of $\sim 0.2\ M_\odot$. A more complete treatment of the effects of reddening and the cluster mass function will be presented in a future paper.

4.5. *Binary Population*

What statements can be made about the binary population? None of the visual binaries listed in Table 6 had previously been identified as such; many had been considered to be single objects in the best previous ground-based observations of the

[3] The difference between the values of $(m - V)_V$ and $(m - M)_I$ is of course because these are the apparent distance moduli.

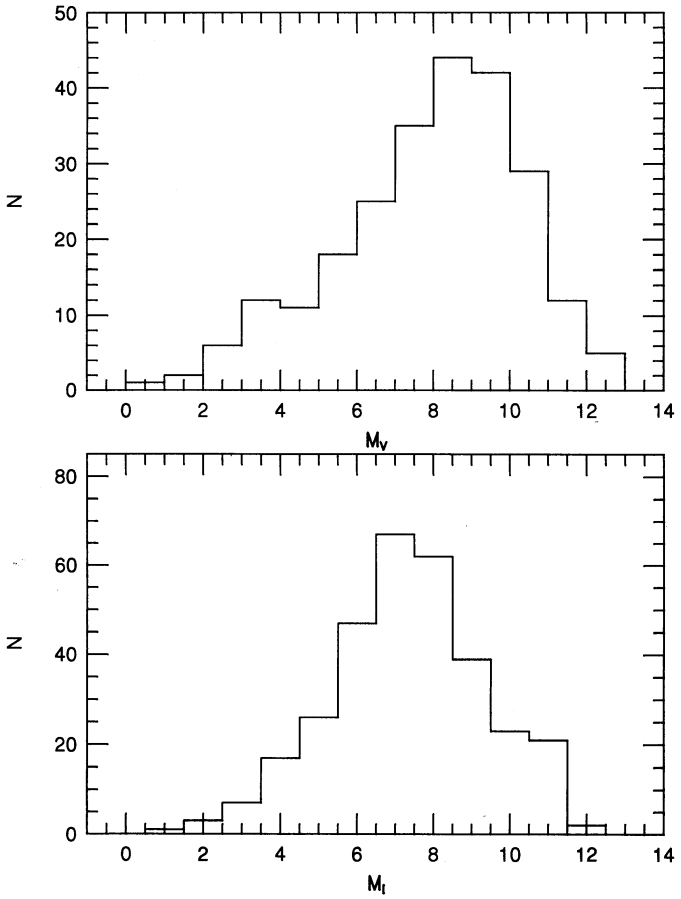

FIG. 13.—Luminosity functons for Trapezium stars observed by *HST*

region (Jones & Walker 1988; Herbig & Terndrup 1986). The observed distribution of separations from the 35 systems in Table 6 are tabulated in Table 9. The pair PC 34/33 (JW 399) was observed twice and while the two observations of the primary are consistent, the magnitudes found for the secondary are different by more than 1.5 mag in V and 0.5 mag in I—perhaps indicating that the secondary is variable or that it was undergoing a flare event. At the present time, we adopt the fainter, redder magnitude for the secondary, PC 33.

To test what fraction of the visual binaries in Table 6 represent chance alignments, we calculated random spatial distributions for the same number of total stars distributed over the same fields observed by *HST*. From 100 such random distributions we found that the average separation distribution would have a total of ~three or four pairs of stars with separations ≤ 1 arcsec. In Figure 14, we plot the observed separation distribution of the *HST* sample, and an average distribution from the 100 random spatial distributions. The peak in the observed sample at separations ≤ 1 arcsec is not seen in a random situation, suggesting that most of the close visual binaries in Table 6 are in fact real binary systems.

TABLE 9

VISUAL BINARY SEPARATIONS

Separation	N
0.″0–0.″1	4
0.1–0.2	6
0.2–0.3	4
0.3–0.4	4
0.4–0.5	6
0.5–0.6	2
0.6–0.7	2
0.7–0.8	0
0.8–0.9	0
0.9–1.0	3
≥ 1.0	4

We illustrate in Figure 15 the locations of the primary and secondary components to the visual binaries listed in Table 6. The three instances of binary systems with blue secondaries have been discussed in § 4.2.

Zinnecker (1989) notes that among a sample of PMS binaries in the Taurus-Auriga region, in most cases the primary was found to be redder than the secondary. Zinnecker suggests a few causes for this which involve the presence of circumstellar disks around one or both stars. Zinnecker's sample consists of a set of T-Tauri binaries with linear separations of 300–1800 AU—much larger than the separation range covered in Table 6. In contrast to the Taurus-Auriga sample of Zinnecker, most primaries in Table 6 are bluer than their secondaries, at least for the separation range discussed here. From the model calculations above, we may expect on the order of 3 or 4 visual binaries with separations $\leq 1''$ to occur due to chance alignments—implying that perhaps some of the close binaries in Table 6 with redder primaries (i.e., blue secondaries) can be explained in this manner. Based on the large number of stars along the cluster locus however, one would predict that most chance alignments should occur between two stars falling along the cluster locus rather than between a star along the cluster locus and one lying off or below it. A remaining possible explanation for some of the systems with redder primaries is the presence of circumstellar disks, as theorized for the Taurus sample.

How does the observed frequency of visual binaries compare to what we would expect for a random sample of field stars? We have searched for binaries with angular separations of about 0.1 to 1.0 arcsec, corresponding to minimum linear separations of about 44 to 440 AU at the distance to the Trapezium cluster. The total number of binary systems we have found in the Trapezium is 35, and if the binary fraction is defined as the number of primary stars divided by the number of single stars plus the number of primaries, then our observed binary fraction is 12%. From the results of the random spatial distribution analysis, if we further say that four of the visual binary systems are chance alignments, then the observed binary fraction is reduced to ~11%. The average system mass for these binaries is likely to be about 1 $M_\odot$, and therefore these linear separations correspond approximately to log $P \simeq 5.0$ to 6.5 days (~275 to 8700 yr). In the Duquennoy & Mayor (1991) G dwarf survey, after correcting for incompleteness they derive a total binary fraction of about 61%, of which 20% are in the period range to which we are sensitive. therefore, according to the Duquennoy & Mayor (1991) study, the total fraction of stars that are binaries in our period range should be $0.61 \times 0.20 = 0.12$, the same as we have found in the Trapezium. Our binary frequency number for the Trapezium, however, was calculated much more crudely than in the Duquennoy & Mayor study, so we do not claim too strongly that the frequencies are identical—only that the two frequencies are not greatly different, and thus that there is no

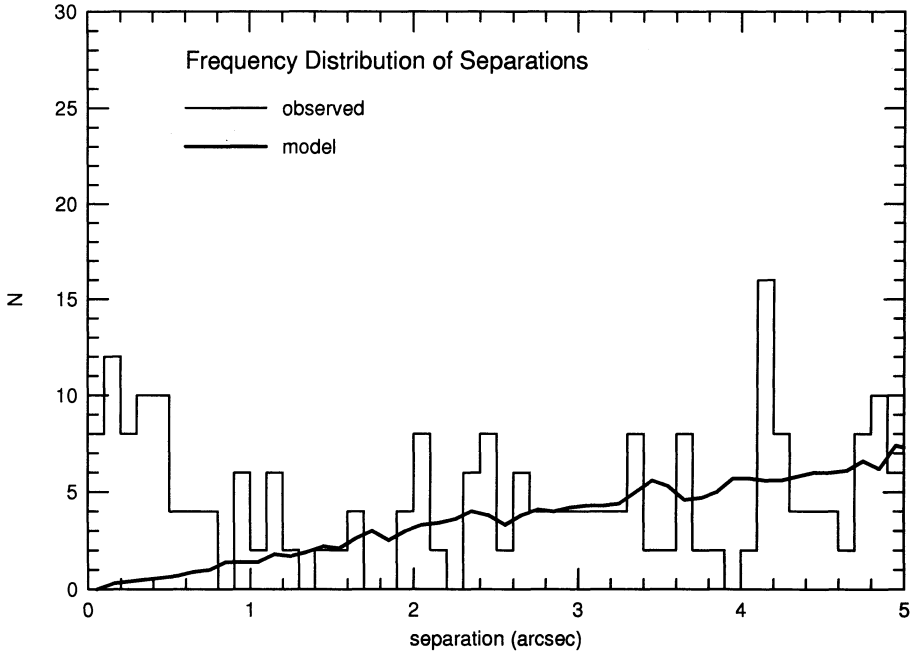

FIG. 14.—Frequency distribution of separations for the Trapezium stars observed by *HST* (*histogram*) and for the average of 100 random spatial distributions (*heavy line*). "N" here is the total number of instances occurring at a given separation for all stars—and therefore represents twice the actual number of pairs of stars at that separation. The comparison between the average random model and the observed distributions indicate an increased frequency at small separations ($< 1''$) in the observed distribution, suggesting that many of the observed visual binaries with small separations are real systems.

evidence that the binary frequency (of stars in our period range) in the Trapezium is unusual.

There are at least two possible interpretations of this result. At one extreme, if one assumes that most stars are formed in rich clusters (Lada et al. 1991), then the similarity of the Trapezium and field binary frequencies is simply a requirement of the hypothesis. At the other extreme, the more traditional view has been that only of order one-tenth of the stars in the Galactic disk are formed in clusters (cf. Miller & Scalo 1978). If that is correct, then the similarity of the field and Trapezium binary frequencies suggests that the mechanism which forms binaries (at least in the separation range to which we are sensitive) is

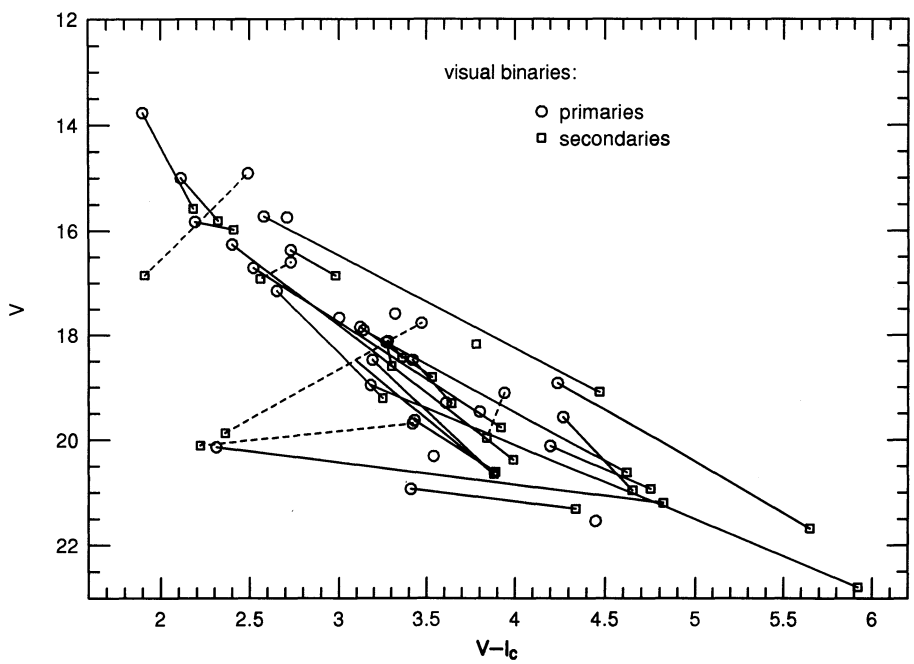

FIG. 15.—Locations in the V vs. $V-I$ diagram of the primary and secondary stars comprising the visual binaries in Table 6. Visual pairs with redder secondaries are connected with solid lines, while those with bluer secondaries are connected with a dashed line. In addition to the three cases of bluer secondaries discussed in § 4.2, the two marginal cases (PC 173/172, PC 224/222) with color differences on the order of the photometric errors are also indicated.

not a function of the large-scale environment in which the binary is formed. Specifically, capture processes—with or without the mediation of disks—would seem to be excluded by this interpretation of our results. This is particularly true because the separation range we are sensitive to is precisely the range in separation distances where at least the disk-mediated capture process should be most efficient (i.e., of order the expected disk size, a few hundred AU, Larson 1990).

4.6. *Nonstellar Objects, Comparison to Radio Sources*

Three interesting cases of nebulosity apparently associated with a stellar source were found from the HST observations. These instances of "nonstellar objects" are designated as PC 160 (=JW 532), PC 190 (=JW 558), and PC 211 in Table 4. Due to the nearby nebulosity, the aperture photometry for the nonstellar objects was estimated by using a larger background aperture region which did not contain the nebulosity near the star. The measured magnitudes were then transformed onto the original aperture photometry system using a set of calibration stars. For PC 211 no real stellar core could be distinguished in V and therefore only an upper limit is quoted in Table 4. The aperture photometry of PC 190 placed it at a bluer $V-I$ color than most stars of similar V magnitudes (Fig. 8)—and is suggestive of additional absorption in V for this star (due to the surrounding nebulous material). The derived aperture photometry for these nonstellar objects remains only approximate, as the surrounding nebulosity likely still influences the magnitudes obtained.

All three nonstellar objects have been detected as compact radio sources by Felli et al. (1993a). Felli et al. find an extended source of 2 cm radio emission corresponding to PC 190 (JW 558).[4] The extended source seen in their Figure 8*b* appears to correspond in shape and orientation to the nebulosity seen in the V and I PC images. While the nebulosity is in all likelihood associated with the stellar component embedded in it, the excitation of the nebulosity may be due to θ^1C rather than the embedded star. In fact, in all three cases noticed here, the nebulosity is oriented or located toward the direction of θ^1C, the primary source of UV photons in the cluster. All three stars are located at approximately the same distance from θ^1C; the projected separations for PC 190 and PC 211 being $\sim 23''$ (0.050 pc), while that for PC 160 is $\sim 36''$ (0.077 pc). O'Dell et al. (1993) resolved 12 similar nebulous objects in the Trapezium cluster using the *HST* WF camera and narrow-band filters centered on emission lines. They also noted the concentration of objects near θ^1C, the orientation of the nebulosity toward θ^1C, and proposed that the compact nebulae are bow shocks produced by ionized gas from protoplanetary disks interacting with the stellar wind from θ^1C. This model was originally proposed to explain these objects based on their characteristics as deduced from ground-based observations (Churchwell et al. 1987; Garay et al. 1987; Laques & Vidal 1979). The contribution of *HST* has been to resolve these sources in the optical and to show that their morphology agrees with the basic model. Further discussion of three sources with compact circumstellar nebulosity is provided in Stauffer et al. (1994).

In Table 10 we list those compact radio sources of Felli et al. which fall within the areas imaged by the PC. The columns in Table 10 list the radio source designation from Felli et al., the identification of any star at or near the radio position, and explanatory notes. In Figure 16 we provide an expanded view of the central Trapezium region, overlaying stellar positions of

TABLE 10

RADIO SOURCES WITHIN PLANETARY CAMERA IMAGES

Radio Source	Star	Notes
Q	...	no object seen
R	PC55=JW432	no nebulosity seen
B	...	possible object (= position of BN object[1])
C	...	nebulous on PC images
H	...	possible object
I	...	possible object (= position of IRc2[1])
D	...	possible object
K	PC143/144= JW519ab	likely ID, no nebulosity seen
M	...	nebulous on PC images
E	PC160=JW532	star with nebulosity
L	PC174=JW548	no nebulosity seen
1	PC190=JW558	star with nebulosity
G	PC207=JW567	near CCD edge, no obvious nebulosity
19	PC211	star with nebulosity
N	PC216=JW581	no nebulosity seen
O	...	nebulous on PC images
F	PC226=JW589	no nebulosity seen
P	PC254=JW622	no nebulosity seen

[1]Downes et al. 1981.

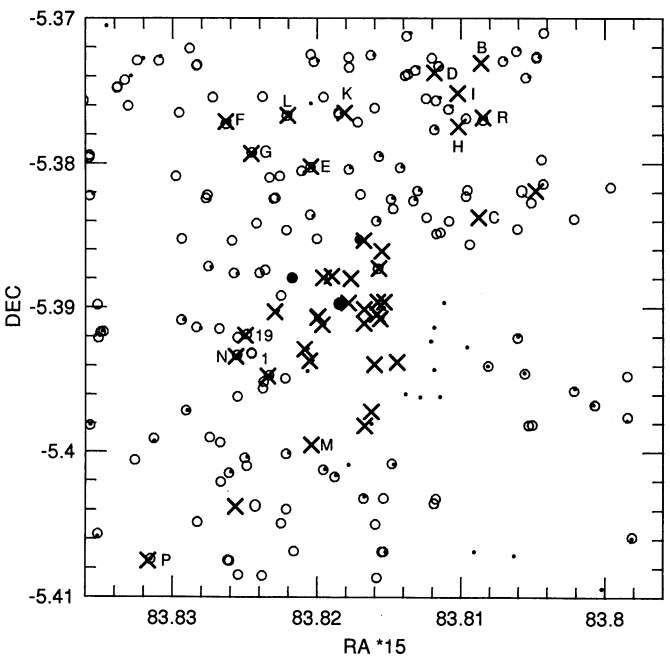

FIG. 16.—Locations of compact radio sources in the central Trapezium region. A few bright stars and JW and PC stars are indicated with the same symbols as in Fig. 5, The radio source positions are indicated with crosses. Those sources falling within the areas imaged by the PC are identified by the designations from Felli et al. Radio sources C, M, and O correspond to regions of enhanced nebulosity in the PC images, Sources B, H, and I may correspond to objects at the limit of the PC images, while no apparent object could be seen at the location of source Q.

[4] In a more recent paper, Felli et al. (1993b) state that no star is present at the position of radio source 1. However, they were apparently not familiar at the time with the existence of the Jones & Walker (1988) survey.

Figure 6 with the radio source positions in the region. For those 18 radio sources in Table 10 falling within the areas observed by this program, we find three associated with the nonstellar objects mentioned above, seven associated with stars for which no apparent nebulosity could be detected on the V and I frames, and three radio sources coincident with apparently dense enhancements of nebulosity. For the remaining radio sources, either no apparent object was seen on the PC images at that position, or a possible stellar object was detected at the limit of the long exposure I frames. For the "possible objects" in Table 10, there was a suggestion of a slight enhancement above background near the radio position—possibly due to the sharply peaked core of a stellar PSF. The fact that no apparent nebulosity was found in some cases of a radio source being associated with a star, should not be taken as conclusive evidence that there is no nebulosity involved. Some of the stars involved are fairly bright, making the detection of any low surface brightness nebulosity near the star difficult due to the stellar PSF. (Deconvolutions of these star images were also attempted, but no associated nebulosity was apparent in the deconvolved images.) The three instances of star + nebulosity found are also among the closest to the possible irradiation source θ^1C, suggesting that the brightness (in medium and wide-band filters at least) of any associated nebulosity may be dependent on the distance from θ^1C.

In Figure 17, we illustrate the location of the so-called "proplyd" objects reported by O'Dell et al. (1993) relative to the PC, JW, and radio source positions. Among the three star+nebulosity objects we see, PC 190 (=JW 558) is the only one in common with O'Dell et al. (their object 1).[5] Object 16 (=JW 588) of O'Dell et al. was not regarded as unusual by us prior to O'Dell et al.'s results; a check of our images reveals no obvious nebulosity. However, this may not be surprising if JW 588 possesses a neutral disk of gas and dust as proposed by O'Dell et al. Some slight additional absorption relative to background may possibly be seen in our V band images, the same as mentioned by O'Dell et al. using the F555W filter. Object 12 of O'Dell et al. corresponds to the star PC 178: this star falls near the edge of our frame, no reliable V mag. could be measured, and no obvious nebulosity was detected in our frames. Object 9 of O'Dell et. al. is recovered in our data as PC 254 (=JW 622; radio source "P") and no nebulosity is seen in our frames. Objects 10 and 17 of O'Dell et al. are seen on the PC images as nebulous features—no stellar core is seen. They are essentially similar to the nebulous patches seen at the radio source positions "M" & "C" (object 10 in fact corresponds to radio source "O").

[5] With the higher resolution provided by the PC, we have been able to detect the central star to JW 558, which O'Dell et al. were unable to resolve.

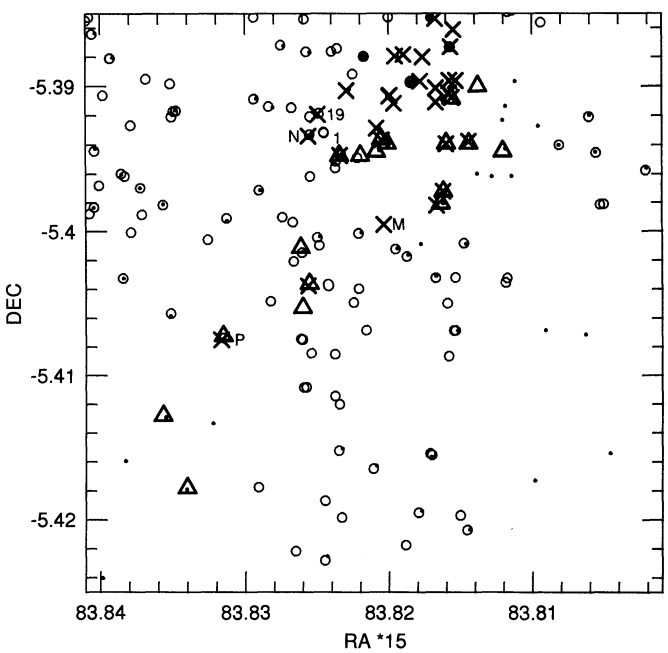

FIG. 17.—Locations of objects given in O'Dell et al. (1993), relative to stars from this survey and JW, and radio sources from Felli et al. (1993a). Symbols are the same as Fig. 16, with the addition of triangles to represent the O'Dell et al. objects.

5. CONCLUSIONS

As noted by HT, the Trapezium cluster is ~100 times denser than typical nearby open clusters. This suggests that it is either an exceedingly rare type of cluster or that it will evolve to become considerably less dense during the next 10–30 Myr. The recent discovery of a few similar, though somewhat less dense, embedded clusters in L1630 and L1641 (Lada et al. 1991; Strom et al. 1993) lends support to the idea that the Trapezium cluster may not be a rare phenomenon, and thus that it is likely to evolve to lower density. Simple theoretical models predict that embedded clusters will expand when the gas cloud from which they are born dissipates (Mathieu 1983; Lada, Margulis, & Dearborn 1984); the amount of expansion depends on the relative mass of the stars and gas on the timescale over which the gas is removed. If that mechanism were used to predict the expansion of the Trapezium cluster, then the current epoch would have to be immediately post-ejection of the gas and prior to the readjustment of the cluster radius since the cluster is no longer embedded and the mass in gas interior to 2 arcmin from θ^1 Ori is not likely to be a significant fraction of the mass in stars. In that event, the cluster would not be in virial equilibrium at this time, but instead would have a velocity dispersion larger than predicted for the observed mass in stars. Jones & Walker (1988) have noted that this is indeed what is observed—the virial mass predicted for the Trapezium cluster from the proper motion measurements is about 2000 $M_\odot$, whereas the mass in stars as counted by HT is only of order 200 $M_\odot$. We have added ~220 more stars than had been observed by HT, but the added total stellar mass is small since these are all low-mass stars. The crucial data still required to determine whether the Trapezium cluster is bound or not are (1) a large area, K band imaging survey of the vicinity of the Trapezium, in order to determine whether the Trapezium cluster is a distinct entity or just the visible portion of a more extended cluster, and (2) a determination of the individual reddening to the Trapezium stars, in order to allow conversion of our luminosity function into a mass function and to indicate whether by going fainter we are simply picking up more embedded stars (and thus, perhaps, not true members of the cluster) rather than lower mass stars.

For a variety of reasons, it would be interesting to measure the properties of the stars in a 10^6 year old, proto-open cluster. Even if the Trapezium cluster is not bound, it is arguably the closest thing we know of to being such a proto-open cluster. Two of the conclusions we have reached based on the *HST* data are notable in this regard. First, we have shown that the age spread of the stars within the Trapezium cluster is small—

80% of the stars have ages less than 10^6 years. If this age spread is representative of typical open clusters, then attempts to explain lithium abundance or rotational velocity dispersions among the low-mass stars in clusters like the Pleiades are excluded (cf. Soderblom et al. 1993). Second, we have shown that the binary frequency for separations of order 40 to 400 AU is essentially the same in the Trapezium cluster as in the field. This argues against capture processes as the agent for forming such binaries. After sufficient reddening data is collected for the *HST* stars, it will be possible to determine the mass function for the Trapezium cluster—which can be compared to the mass function for T associations in order, for example, to test bimodial star-formation models.

Comparison to FJS's tracks suggests a median age of $\sim 3 \times 10^5$ yr, a value which is uncertain due to the importance of deuterium burning. Perhaps more importantly, the Trapezium stars lie above almost all of the Taurus pre–main-sequence stars in the HR diagram (cf. Gomez et al. 1993). Thus, it appears that the dense environment of the Trapezium not only produced stars faster than Taurus, but also formed stars higher in the HR diagram, i.e., with a higher "birthline" (Stahler 1988). Stahler (1988) showed that the position of the "birthline" moves somewhat upward with higher stellar accretion rates (the effect is limited by deuterium burning). This leads us to suggest that the Trapezium region, with its high initial density, produced more rapid accretion into stars.

It is interesting to speculate what HST images would be able to show in the region of the Trapezium if the aberration errors in the primary mirror were removed. Our images, and those of O'Dell et al., have shown the existence of circumstellar matter around some of the Trapezium stars with size scales of a few hundred AU. The repaired *HST* should be able to extend these types of studies to considerably fainter and smaller features, and thus should provide both more detailed images of the already identified sources and a better census of the ubiquity of these types of structures. If these are disks, it will be useful to compare their properties versus those measured for T Tauri stars in associations. It will also be useful to search for such circumstellar nebulosity in stars identified as visual binaries in our images—one might expect that the disks in such binaries would be absent or truncated. With improved optics, the *HST* images could again go fainter than currently possible, perhaps even reaching the brown dwarf luminosity range (assuming brown dwarfs exist).

Support for this work was provided by NASA through grant number GO2595.0 1-87A from the Space Telescope Science Institute, which is operated by the Association of Universities for Research in Astronomy, Inc., under NASA contract NAS5-26555. We would like to thank G. Herbig for providing a copy of VandenBerg's theoretical models used in HT and Fritz Swenson for providing his theoretical models prior to publication. Discussions by one of us (C. P.) with C. Burrows, A. Saha, J. MacKenty, and E. Wyckoff at STScI regarding WFPC reductions were very helpful. Early advice and comments on WFPC reductions from Jon Holtzmann are appreciated.

APPENDIX

The issues and questions revolving around the accurate transformation between colors and effective temperatures at cool temperatures is deserving of a paper in itself; in this appendix we only illustrate various color-temperature relations for the low temperature regime that is encountered in analysis of the *HST* data. In Figure 18, we have chosen the $V-I$(Kron) color to plot against effective temperature to illustrate the various relations. Shown in the figure are (1) the relation determined from a

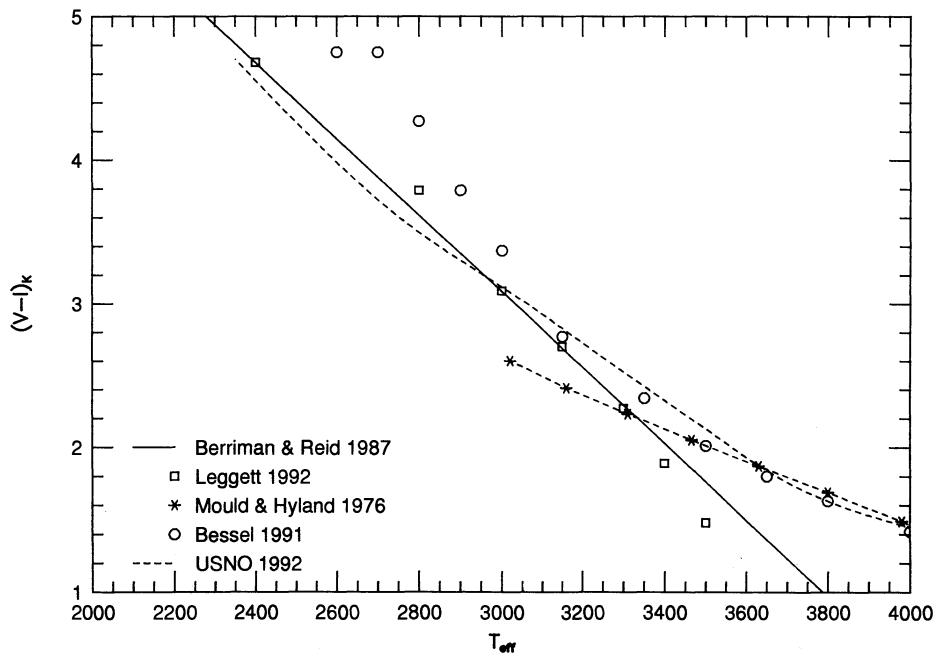

FIG. 18.—Plot of various $V-I$(Kron) vs. $T_{\rm eff}$ relations discussed in the Appendix

least-squares fit to the results of Berriman & Reid (1987) (their results were recently reconfirmed by Berriman, Reid, & Leggett 1992); (2) the relation tabulated in Table 6 of Leggett (1992) which is also based on the Berriman & Reid (1987) temperature scale; (3) the Mould & Hyland (1976) relation; (4) the relation based on Bessell (1991); and (5) the empirical "USNO" relation shown in Figure 11 of Monet et al. (1992). The tabulation for the USNO relation was provided by C. Dahn. The Bessell relation shown in Figure 18 was derived from transforming the $V-I$(Cousins) colors given in his Table 2 to $V-I$(Kron) using the relation from Bessell & Weis (1987).

At warmer temperatures ($T \geq 3500$ K), the Berriman & Reid (1987) relation is based on fewer data points than the Mould & Hyland (1976) data set, and other than Berriman and Reid, all other relations are essentially consistent with each other in the warm temperature regime of Figure 18. Cooler than 3300 K, the Mould and Hyland relation is seen to depart from the relations of Berriman and Reid, Bessel, and USNO. This difference between MH and the other relations becomes more and more significant as one goes to cooler temperatures; reaching ~ 0.5 in $V-I$ at $T_{\rm eff} \simeq 3000$ K.

The following description outlines our best estimate of the color-temperature relation employed in the present paper. For $\log T_{\rm eff} > 3.62$, we have used FJS's $B-V$ tabulated values to obtain $V-I$(Kron) using a color-color relation derived from the field star photometry of Kron, Gascoigne, & White (1957). Using the transformation relation from Bessell & Weis (1987), the $V-I$(Kron) colors were converted into $V-I$(Cousins) colors. (We note that it would be convenient if $V-I$ colors in the Kron and the Cousins systems could be tabulated in addition to $B-V$ in evolutionary models.) For $\log T_{\rm eff} < 3.62$, $T_{\rm eff}$ was transformed to $R-I$(Kron) using the relation tabulated in Mould & Hyland (1976). The $R-I$ value was again transformed to $V-I$(Kron) using the Kron field standards, and transformed to $V-I$(Cousins) using the Bessell & Weis (1987) relation. For temperatures ≤ 3300 K ($\log T_{\rm eff} \leq 3.5185$), we choose to employ the relation derived from Berriman & Reid (1987, hereafter BR) as a better estimate than Mould & Hyland (1976, hereafter MH). The BR relation yielded $V-I$(Kron) colors which were then converted to the Cousins system as above. In order to make the transition between $\log T_{\rm eff} > 3.62$ and $\log T_{\rm eff} < 3.62$ more continuous, a small correction was applied to the MH and BR colors: $\Delta(V-I) = -0.05$.

REFERENCES

Adams, M. T., Strom, K. M., & Strom, S. E. 1983, ApJS, 53, 893
Baade, W., & Minkowski, R. 1937, ApJ, 86, 119
Balachandran, S., Lambert, D. L., & Stauffer, J. R. 1988, ApJ, 333, 267
Berriman, G., & Reid, N. 1987, MNRAS, 227, 315 (BR)
Berriman, G., Reid, N., & Leggett, S. K. 1992, ApJ, 392, L31
Bessell, M. S. 1979, PASP, 91, 589
———. 1991, AJ, 101, 662
Bessell, M. S., & Weis, E. W. 1987, AJ, 99, 642
Burrows, C. 1992, private communication
Churchwell, E., Felli, M., Wood, D. O. S., & Massi, M. 1987, ApJ, 321, 516
Clarke, C., & Pringle, J. 1991a, MNRAS, 249, 584
———. 1991b, MNRAS, 249, 588
Cohen, M., & Kuhi, L. V. 1979, ApJS, 41, 743
Downes, D., Genzel, R., Becklin, E. E., & Wynn-Williams, C. G. 1981, ApJ, 244, 869
Duquennoy, A., & Mayor, M. 1991, A&A, 248, 485
Felli, M., Churchwell, E., Wilson, T. L., & Taylor, G. 1993a, A&AS, 98, 137
Felli, M., Taylor, G. B., Catarzi, M., Churchwell, E., & Kurtz, S. 1993b, A&AS, 101, 127
Gagne, M., et al. 1993, private communication
Garay, G., Moran, J. M., & Reid, M. J. 1987, ApJ, 314, 535
Gilmozzi, R. 1990, Instrument Science Report WFPC 90-007 (Baltimore: STScI)
Gomez, M., Hartmann, L., Kenyon, S. J., & Hewett, R. 1993, AJ, 105, 1927
Heller, C. H. 1993, ApJ, 408, 337
Herbig, G. H. 1982, in Symp. on the Orion Nebula to Honor Henry Draper, ed. A. E. Glassgold & P. J. Huggins (New York: New York Acad. Sci.), 64
Herbig, G. H., & Terndrup, D. M. 1986, ApJ, 307, 609 (HT)
Holtzmann, J. A., et al. 1991, ApJ, 369, L35
———. 1994, in preparation
Iben, I., Jr., & Talbot, R. J. 1966, ApJ, 144, 968
Jones, B. F., & Walker, M. F. 1988, AJ, 95, 1755 (JW)
Kenyon, S. J., & Hartmann, L. W. 1990, ApJ, 349, 197
Kron, G., Gascoigne, S., & White, H. 1957, AJ, 62, 205
Kroupa, P., Gilmore, G., & Tout, C. A. 1992, AJ, 103, 1602
Lada, C., Margulis, M., & Dearborn, D. 1984, ApJ, 285, 141
Lada, E., Depoy, D., Evans, N., & Gatley, I. 1991, ApJ, 371, 171
Laques, P., & Vidal, J. L. 1979, A&A, 73, 97
Larson, R. 1990, in Physical Processes in Fragmentation and Star Formation, ed. R. Capuzzo-Dolcetta, C. Chiosio, & A. Fazio (Dordrecht: Kluwer), 389
Leggett, S. K. 1992, ApJS, 82, 351
Leous, J. A., Feigelson, E. D., André, P., & Montmerle, T. 1991, ApJ, 379, 683
Mathieu, R. 1983, ApJ, 267, L97
McCaughrean, M., et al. 1994, in preparation
Meaburn, J., Massey, R. M., Raga, A. C., & Clayton, C. A. 1993, MNRAS, 260, 625
Miller, G. E., & Scalo, J. M. 1978, PASP, 90, 506
Monet, D. G. 1991, in WF/PC Final Orbital/Science Verification Report, ed. S. M. Faber (Baltimore: STScI), chap. 7
Monet, D. G., Dahn, C. C., Vrba, F. J., Harris, H. C., Pier, J. R., Luginbuhl, C. B., & Ables, H. D. 1992, AJ, 103, 638
Montmerle, T., Koch-Miramond, L., Falgarone, E., & Grindlay, J. 1983, ApJ, 269, 182
Mould, J. R., & Hyland, A. R. 1976, ApJ, 208, 399 (MH)
O'Dell, C. R., Wen, Z., & Hu, X. 1993, ApJ, 410, 696
Parenago, P. P. 1954, Trudy Sternberg Astron. Inst. 25
Prosser, C. P. 1992, AJ, 103, 488
Rieke, G. H., Low, F. J., & Kleinmann, D. E. 1973, ApJ, 186, L7
Soderblom, D. R., Jones, B. F., Balachandran, S., Stauffer, J. R., Duncan, D. K., Fedele, S., & Hudon, J. D. 1993, AJ, 106, 1059
Stahler, S. W. 1985, ApJ, 293, 207
———. 1988, ApJ, 332, 804
Stauffer, J. R., & Hartmann, L. 1986, ApJS, 61, 531
———. 1987, ApJ, 318, 337
Stauffer, J. R., et al. 1994, in preparation
Stetson, P. B. 1987, PASP, 99, 91
Strom, K. M., Strom, S. E., Edwards, S., Cabrit, S., & Strutskie, M. F. 1989, AJ, 97, 1451
Strom, K. M., Strom, S. E., & Yost, J. 1971, ApJ, 165, 479
Strom, S. E., et al. 1993, preprint
Swenson, F. J., Faulkner, J., Rogers, F. J., & Iglesias, C. A. 1994, ApJ, submitted (FJS)
Trümpler, R. 1931, PASP, 43, 255
VandenBerg, D. A. 1984, unpublished
———. 1987, unpublished
———. 1992, ApJ, 391, 685
Warren, W. H., & Hesser, J. E. 1978, ApJS, 36, 497
Werner, M. W., Gatley, I., Harper, D. A., Becklin, E. E., Loewenstein, R. F., Telesco, C. M., & Thronson, H. A. 1976, ApJ, 204, 420
Wynn-Williams, C. G., & Becklin, E. E. 1974, PASP, 86, 5
Zinnecker, H. 1989, in ESO Conf. Proc. 33, Low-Mass Star Formation and Pre–Main-Sequence Objects, ed. B. Reipurth (Munich: ESO), 447
Zinnecker, H., McCaughrean, M., & Wilking, B. 1992, in Protostars and Planets III, ed. E. Levy, J. Levine, & M. Matthews (Tucson: Univ. Arizona Press), 429